

1 **Dynamic Processes Dominating Ozone Variability**  
2 **Induced by Synoptic Weather Patterns in Warm Seasons**  
3 of 2014–2018 over the Yangtze River Delta Region, China

4 Da Gao<sup>1</sup>, Min Xie<sup>1\*</sup>, Jane Liu<sup>2,3</sup>, Tijian Wang<sup>1</sup>, Chaoqun Ma<sup>1,a</sup>, Haokun Bai<sup>1</sup>, Xing Chen<sup>1</sup>, Junyu  
5 RenMengmeng Li<sup>1</sup>, Bingliang ZhuangYangzhihao Zhan<sup>1</sup>, Shu Li<sup>1</sup>

6 <sup>1</sup> School of Atmospheric Sciences, Joint Center for Atmospheric Radar Research of CMA/NJU,  
7 CMA-NJU Joint Laboratory for Climate Prediction Studies, Jiangsu Collaborative Innovation  
8 Center for Climate Change, Nanjing University, Nanjing 210023, China

9 <sup>2</sup> College of Geographic Sciences, Fujian Normal University, Fuzhou 350007, China

10 <sup>3</sup> Department of Geography and Planning, University of Toronto M5S 3G3, Canada

11 <sup>a</sup> now at: Minerva Research Group, Max Planck Institute for Chemistry, Mainz, Germany

12 -----

13 \* Corresponding author. School of Atmospheric Sciences, Nanjing University, Nanjing 210023,  
14 China. minxie@nju.edu.cn (M. Xie)

15

16 **Abstract:** Ozone ( $O_3$ ) pollution is of great concern in the Yangtze River Delta (YRD) region of  
17 China, and the regional  $O_3$  pollution is closely associated with dominant weather systems. With a  
18 focus on the warm seasons (April–September) from 2014 to 2018, we quantitatively analyze the  
19 characteristics of  $O_3$  variations over the YRD, the impacts of large-scale and synoptic-scale  
20 circulations on the  $O_3$  variations and the associated meteorological controlling factors, based on  
21 observed ground-level  $O_3$  and meteorological data. Our analysis suggests an increasing trend of the  
22 regional mean  $O_3$  concentration in the YRD at 1.81 ppb per year over 2014–2018. Spatially, the  
23 empirical orthogonal function (EOF) analysis suggests the dominant mode accounting for 65.70%  
24 variation in  $O_3$ , implying that an increase in  $O_3$  is the dominant tendency in the entire YRD.  
25 Meteorology is estimated to increase the regional mean  $O_3$  concentration by 3.032.84 ppb at most  
26 from 2014 to 2018. Especially, compared to solar radiation (SR) and low cloud cover (LCC) of  
27 relatively large impacting on  $O_3$  variation, relative humidity (RH) plays the most important role in  
28 modulating the inter-annual  $O_3$  variation–Relative humidity is found to be the most influential  
29 meteorological factor impacting  $O_3$  concentration. As the atmospheric circulations can affect local

30 meteorological factors and O<sub>3</sub> levels, we identify five dominant synoptic weather patterns (SWPs)  
31 in the warm seasons in the YRD using the t-mode principal component analysis (PTT) classification.  
32 The typical weather systems of SWPs include the western Pacific Subtropical High (WPSH) under  
33 SWP1, a continental high under SWP2, an extratropical cyclone under SWP3, a southern low  
34 pressure and WPSH under SWP4 and the north China anticyclone under SWP5. The annual  
35 variations of the all five SWPs are all favorable to the increase in O<sub>3</sub> concentrations over 2014–  
36 2018. However, crucial meteorological factors leading to increases in causing increasing of O<sub>3</sub>  
37 concentrations are different under different each SWP. These factors are identified as, including  
38 significant decreases in decreasing relative humidity RH and increases in, strengthening SR solar  
39 radiation under SWPs 1, SWP4 and SWP5, significant decreases in RH, increases  
40 in strengthening SR and increasing air temperature (T2) under SWP2, and significant decreases in RH  
41 under SWP3. Under SWPs 1, 4 and 5, significant decreases in decreasing RH and increases  
42 in strengthening SR are predominantly caused by the WPSH weakening and northward extending  
43 under SWP1, the southern low pressure weakening and the WPSH weakening under SWP4, and the  
44 north China anticyclone weakening under SWP5. Under SWP2, significant decreases in  
45 decreasing RH, increases in strengthening SR and increasing T2 are mainly chiefly  
46 produced by a continental high weakening. Under SWP3, significantly decreasing RH  
47 is mainly induced by an extratropical cyclone strengthening. These changes in atmospheric  
48 circulations prevent the water vapor in the southern and northern sea from being transported to the  
49 YRD and result in RH sSignificantly decreasing under each SWP. In addition, strengthened  
50 descending motions (behind the strengthening trough and in front of the strengthening ridge) lead  
51 to decreases in LCC and sSignificantly strengthening SR under SWP1, 2, 4 and 5. The  
52 sSignificantly increases in T2 would be due to weakening cold flow introduced by a weakening  
53 continental high. Moreover, Most importantly, the the these changes in in the SWP intensity can  
54 make large variations in causing significant meteorological factors and contribute more variation  
55 take more contributions more to the O<sub>3</sub> inter-annual variation than the variation in the SWP  
56 frequency change. The SWP intensity change includes the weakening and northward extending  
57 of the western Pacific subtropical high (WPSH) under SWP1, the weakening of the continental high  
58 under SWP2, an extratropical cyclone strengthening under SWP3, the southern low pressure

带格式的: 非突出显示

59 ~~weakening and WPSH weakening under SWP4, and the north China anticyclone weakening under~~  
60 ~~SWP5. All these changes prevent the water vapor in the southern sea from being transported to the~~  
61 ~~YRD, and increase air temperature in the YRD. In addition, the descending motions strengthen in~~  
62 ~~the YRD located behind the trough and in front of the ridge due to the strengthening of the ridge~~  
63 ~~and trough in the westerlies. Then, the strengthened descending motion leads to less cloud cover~~  
64 ~~and strong solar radiation, which are favorable to O<sub>3</sub> formation and accumulation.~~ Finally, we  
65 reconstruct an EOF mode 1 time series that ~~is shows~~ highly correlated with the original O<sub>3</sub> time  
66 series, and the reconstructed time series performs well in defining the change in SWP intensity  
67 according to the unique feature under each of the SWPs.

68

## 69 1. Introduction

70 As an air pollutant, surface ozone (O<sub>3</sub>) is harmful to human health and vegetation growth, such  
71 as damaging human lungs (Jerrett et al. 2009; Day et al. 2017) and destroying forest and agricultural  
72 crops (Yue et al. 2017). ~~A~~In recent years, after the reducing the emission controls following  
73 “Thirteenth Five-Year Plan” Comprehensive Work Plan for Energy Saving and Emission Reduction  
74 in China since 2016, concentrations of many pollutants have decreased over the past few years in  
75 China, but not for O<sub>3</sub>. Furthermore, heavy O<sub>3</sub> pollution episodes occur more frequently and more  
76 severely in China than those in Japan, South Korea, Europe and the United States, and the European  
77 countries (Lu et al. 2018). Li et al. (2018) proposed that the rapid decrease of fine particulate  
78 matter (PM) in China is a reason for such O<sub>3</sub> increase as by slowing down the aerosol sinks of hydro-  
79 preoxy radicals are reduced. Yet, the contribution of meteorological influences on factors to the O<sub>3</sub>  
80 increase are is unclear and require needs further investigations.

81 Surface O<sub>3</sub> is mainly formed through complex and nonlinear photochemical reactions of volatile  
82 organic compounds (VOCs) and nitrogen oxides (NO<sub>x</sub>) exposed to the sunlight. Ozone formation is  
83 sensitive to concentrations of NO<sub>x</sub> and VOCs, i.e., O<sub>3</sub> formation can be NO<sub>x</sub> limited or VOC limited  
84 regimes depending on concentrations of NO<sub>x</sub> and VOCs (Xie et al. 2014; Jin and Holloway 2015).  
85 Meteorology canould also affect O<sub>3</sub> levels through modulation of photochemical reactions,  
86 advection, convection and turbulent transport, as well as dry and wet depositions (Liu et al. 2013;  
87 Xie et al., 2016a, 2016b). Synoptic weather patterns (SWPs) and the associated meteorological  
88 conditions can impact long-term and daily O<sub>3</sub> variations (Hegarty et al., 2007; Santurtún et al., 2015;

带格式的: 字体颜色: 文字 1

89 Gao et al., 2020; Shu et al., 2020). Understanding the mechanisms of meteorological influences on  
90 O<sub>3</sub> variations and quantifying such influences would help provide effective emission controlling  
91 plans for to understand the formation of O<sub>3</sub> pollution.

92 Previous studies have revealed that ~~S~~evere O<sub>3</sub> pollution episodes are usually accompanied  
93 with ~~specific local meteorological conditions, such as~~ high temperature, strong solar radiation,  
94 drying condition and stagnant weather ~~etc.~~ (Jacob and Winner 2009; Doherty et al. 2013; Shu et al.  
95 2016; Pu et al. 2017; Zhang et al. 2018), and Moreover, these local meteorological conditions are  
96 often related to specific synoptic-scale and large-scale atmospheric circulation systems (Fiore et al.  
97 2003; Leibensperger et al. 2008; Barnes and Fiore. 2013; Shu et al. 2016; Wang et al. 2016; Zhao  
98 and Wang. 2017 文献). For example, O<sub>3</sub> pollution in the eastern United States is notably influenced  
99 by the cyclone frequency (Leibensperger et al. 2008), latitude of the polar jet over eastern North  
100 America (Barnes and Fiore. 2013) and the behavior of the quasi-permanent Bermuda High (Fiore  
101 et al. 2003<sup>5</sup>; Wang et al. 2016). In China, Yang et al. (2014) illustrated that the changes in  
102 meteorological variable parameters, associated with the East Asian summer monsoon, lead to 2–5 %  
103 inter-annual variations in surface O<sub>3</sub> concentrations over the central-eastern China. Zhao and Wang  
104 et al. (2017) found that a significantly strong western Pacific subtropical high (WPSH) could result  
105 in higher relative humidity (RH), more clouds, more rainfall, and less ultraviolet radiation, finally  
106 leading to less O<sub>3</sub> formation. Using model simulation, Shu et al. (2016) investigated the synergistical  
107 impact of the the WPSH and typhoons on O<sub>3</sub> level pollution in Yangtze River Delta region.

108 As known, a region is influenced by different weather systems. Weather classification, as a way  
109 to distinguish the different large-scale and synoptic-scale atmospheric circulation systems, is widely  
110 used in exploring connections between weather patterns and O<sub>3</sub> levels (Han et al. 2020; Gao et al.  
111 2020). Gao et al. (2020) discussed influences of six SWPs on O<sub>3</sub> levels in the YRD, and revealed  
112 differences in O<sub>3</sub> pollution levels due to the minor changes in atmospheric circulations. However,  
113 spatially, it is uncertain that how the changes in the SWPs could lead to O<sub>3</sub> pollution in detail,  
114 especially in the YRD. For the northern China and the PRD region, Liu et al. (2019) quantified the  
115 impact of synoptic circulation patterns on O<sub>3</sub> variability in the northern China from April to October  
116 during 2013–2017. Yang et al. (2019) quantitatively assessed the impacts of meteorological factors  
117 and the precursor emissions on the long-term trend of ambient O<sub>3</sub> over the PRD region. However Yet,

带格式的: 字体颜色: 文字 1

带格式的: 非突出显示

带格式的: 非突出显示

带格式的: 非突出显示

带格式的: 非突出显示

118 whether variations in SWPs can lead to O<sub>3</sub> increases in recent years over the YRD has not be  
119 sufficiently addressed.

120 Due to the recent increases in ever growing O<sub>3</sub> level over in the YRD (Tong et al. 2017; Gao  
121 et al. 2017; Xie et al. 2017), the studies on characteristiccharacterizing ies of the O<sub>3</sub> variation in the  
122 region and understanding thethe underlying mechanisms for the variation are urgently required. To  
123 this end, here the temporal and spatial variations in surface O<sub>3</sub> including variations in space and  
124 time, as well as 5-year trend over, in the YRD areis quantitatively investigated, and the mechanisms  
125 of meteorological influences on the O<sub>3</sub> variations are analyzed. Especially, the characteristics of the  
126 corresponding SWPs are discussed in detailed. The remainder of this paper is organized as follows.  
127 Data and methods are introduced in section 2. The inter-annual variation and 5-year trend and spatial  
128 variation characteristics of surface ozone in the YRD – are illustrated in section 3.1. The impact of  
129 meteorological factors on the O<sub>3</sub> variation is discussed in section 3.2. The main SWPs and the effects  
130 of their changess on the O<sub>3</sub> variation are described in section 3.3. Section 3.4 discusses the  
131 contributions of the changes in SWP intensity and frequencychange to the inter-annual variation  
132 and trend of O<sub>3</sub>. Finally, the conclusion and discussions are shown in section 4.

133

## 134 **2. Data and methods**

135 **2.1. O<sub>3</sub> and meteorological datasets**

136 The maximum daily 8-hours average O<sub>3</sub> data are available from the National Environmental  
137 Monitoring Center of China, which were acquired from the air quality real-time publishing platform  
138 (<http://106.37.208.233:20035>). The hourly observation data of meteorological factors including air  
139 temperature (T), RH and wind speed (WS) and sunshine duration (SD) in the warm seasons from  
140 April to September over 2014–2018 were acquired from the National Meteorological Center of  
141 China Meteorological Administration (<http://eng.nmc.cn>). 26 cities are selected as typical cities  
142 representative of the YRD according to the “Urban agglomeration on Yangtze River Delta”  
143 approved by China’s State Council in 2016. There are total 172 stations in 26 cities. In order to  
144 better characterize the O<sub>3</sub> pollution levels of each city, the hourly O<sub>3</sub> concentration of each city is  
145 calculated as the average value of the O<sub>3</sub> concentrations measured in several of the national  
146 monitoring sites in that city. In this paper, the term “O<sub>3</sub> concentration” refers to the maximum daily  
147 8-hours average O<sub>3</sub> concentration unless stated otherwise.

带格式的: 非突出显示  
带格式的: 非突出显示  
带格式的: 非突出显示  
带格式的: 非突出显示  
带格式的: 非突出显示

149 **2.2. Linear trend analyses**

150 ~~T~~in order to characterize the O<sub>3</sub> variation in the warm seasons during 2014–2018 over the  
 151 YRD, a linear trend method based on monthly anomalies is used (see Equation 1), which has been  
 152 widely used to calculate the trends of time series with seasonal cycles and autocorrelation.~~—~~ The O<sub>3</sub>  
 153 monthly anomalies are more precise than O<sub>3</sub> monthly means because ~~the impact of of the reducing~~  
 154 ~~impact of~~ missing data ~~is reduced. In addition, hourly O<sub>3</sub> data and fewer yearly O<sub>3</sub> data are~~  
 155 ~~inappropriate to use because of due to the containing too many temporal variation signals and easily~~  
 156 ~~overfitting.~~ Using this method, Cooper et al. (2020) and Lu et al. (2020) quantified the O<sub>3</sub> trend in  
 157 27 globally distributed remote locations and the whole China. ~~A~~In addition, anomalies of monthly  
 158 average O<sub>3</sub> concentration are defined as the difference between the individual monthly mean and  
 159 the monthly mean of 2014–2018. The parametric linear trend is calculated by using the generalized  
 160 least-squares method with auto-regression.

161 
$$y_t = b + kt + \alpha \cos\left(\frac{2\pi M}{6}\right) + \beta \sin\left(\frac{2\pi M}{6}\right) + R_t \quad (1),$$

162 where  $y_t$  represents the monthly anomaly,  $t$  is the monthly index from April to September during  
 163 2014–2018,  $b$  denotes the intercept,  $k$  is the linear trend,  $\alpha$  and  $\beta$  are coefficients for a 6-  
 164 month harmonic series (M ranges from 1 to 6) which is used to account for potentially remaining  
 165 seasonal signals, and  $R_t$  represents a normal random error series. ~~In this study, linear trend  $k$  is~~  
 166 ~~regarded as the inter-annual O<sub>3</sub> variation trend and is discussed in section 3.1.1.~~

167

168 **2.3. Meteorological adjustment**

169 The meteorological adjustment, a statistical method, is applied to quantify the impact of  
 170 meteorology on O<sub>3</sub> variation through removing such impact in the original O<sub>3</sub> data. It is similar to a  
 171 model simulation that keeps the emission levels fixed but allows meteorology to vary. Yet, this  
 172 method requires much less computing resources than a model simulation. The method is introduced  
 173 in detail as follows.

174 In the meteorological adjustment, the observed O<sub>3</sub> and meteorological data are separated into  
 175 long-term, seasonal, and short-term data (Rao and Zurbanenko 1994a, b). The Kolmogorov-Zurbanenko  
 176 (KZ) filter can be expressed as follows.

带格式的: 非突出显示

带格式的: 非突出显示

带格式的: 字体: 倾斜

177  $R(t) = L(t) + S(t) + W(t)$  (2),

178 where  $R(t)$  represents the raw time series data,  $L(t)$  the long-term trend on a timescale of years,  
179  $S(t)$  the seasonal variation on a timescale of months, and  $W(t)$  the short-term component on a  
180 timescale of days.

181 In order to remove the high-pass signal, the KZ filter carries out  $p$  times of iterations of a  
182 moving average with the window length  $m$ , which is defined as

183  $Y_i = \frac{1}{m} \sum_{j=-k}^k R_{i+j}$  (3)

184 where  $R$  is the original time series,  $i$  an index for the time of iteration,  $j$  an index for sampling inside  
185 the window, and  $k$  the number of sampling on one side of the window. The window length  $m = 2k$   
186 + 1.  $Y$  is the input time series after one iteration. Different scales of motions are obtained by changing  
187 the window length and the number of iterations (Milanchus et al. 1998; Eskridge et al. 1997). The  
188 filter periods of less than  $N$  days can be calculated with window length  $m$  and the number of  
189 iteration  $p$ , as follows:

190  $m \times p^{\frac{1}{2}} \leq N$  (4).

191 Therefore, the cycles of 33 days can be removed by a KZ-(15, 5) filter with the window length of  
192 15 and 5 iterations. In ~~Ethe following~~ equation 5,  $BL(t)$  is the  $O_3$  and meteorological time series  
193 obtained by KZ(15,5) filter and refers to their baseline variations which are the sum of the long term  
194  $L(t)$  and the seasonal component  $S(t)$ .

195  $BL(t) = KZ_{(15,5)} = L(t) + S(t) = KZ_{(183,3)} + S(t)$  (5).

196 The long-term trend is separated from the raw data obtained by KZ (183, 3) with the periods of >  
197 632 days, and then the seasonal and the short-term component  $W(t)$  can be defined as

198  $S(t) = KZ_{(15,5)} - KZ_{(183,3)}$  (6),

199  $W(t) = X(t) - BL(t) = X(t) - KZ_{(15,5)}$  (7).

200 After KZ filtering, the meteorological adjustment is conducted by the multivariate regression  
201 between the  $O_3$  concentration and meteorological factors such as T, RH, wind speed and sunshine  
202 duration (Wise and Comrie 2005; Papanastasiou et al. 2012).

203  $A_{BL}(t) = a_{BL} + \sum b_{BLi} \cdot M_{BLi} + \epsilon_{BL}(t)$  (8),

204  $A_W(t) = a_W + \sum b_{Wi} \cdot M_{Wi} + \epsilon_W(t)$  (9),

205  $\epsilon(t) = \epsilon_{BL}(t) + \epsilon_W(t)$  (10),

206  $A_{ad}(t) = \epsilon(t) + \sum b_{BLi} \cdot \bar{M}_{BLi} + \sum b_{Wi} \cdot \bar{M}_{Wi} + a_{BL} + a_W \quad (11)$

207 the multivariate regression models between baseline and short-term O<sub>3</sub> and meteorological factors  
208 are shown in [Equations 8 and 9](#). The  $A_{BL}(t)$  and  $M_{BLi}$  represent the sum of the long term L(t)  
209 and the seasonal component S(t) of O<sub>3</sub> concentration and meteorological factors. The  $A_W(t)$  and  
210  $M_{Wi}$  represent the short-term W(t) of O<sub>3</sub> concentration and meteorological factors. The  $a$  and  $b$   
211 are the fitted parameters, and  $i$  is time point (days).  $\epsilon(t)$  is the residual term. The average  
212 meteorological condition  $\bar{M}$  at the same calendar date during the 5 years is regarded as the base  
213 condition for that date, and the meteorological adjustment is conducted against the base condition.  
214 [InBy](#) these steps,  $A_{ad}(t)$  refers to the meteorologically adjusted O<sub>3</sub> variation with the  
215 homogenized annual variation in meteorological conditions. The difference between raw O<sub>3</sub> time  
216 series and  $A_{ad}(t)$  represents the meteorological impact.

带格式的: 非突出显示

217

#### 218 **2.4. Classification of SWPs**

219 In order to find the detailed variation characteristics of SWPs, we first extract the predominant  
220 SWPs in the warm seasons over the YRD using a weather classification method. Common objective  
221 classification methods include using predefined type, the leader algorithm, the cluster analysis,  
222 optimization algorithms and eigenvectors (Philipp et al. 2016). The PTT method, a simplified  
223 variant of t-mode principal component analysis using orthogonal rotation, is used to classify SWPs  
224 during 2014–2018. It is one of the methods for weather classification in European Cooperation in  
225 Science and Technology Action 733 (Philipp et al. 2016), which is widely used in atmospheric  
226 sciences (Hou et al. 2019).

227

#### 228 **2.5. FNL and ERA-Interim meteorological data**

229 The National Center for Environmental Prediction Final Operational Global Analysis (FNL)  
230 data (<http://rda.ucar.edu/datasets/ds083.2/>) produced by the Global Data Assimilation System are  
231 used in classifying SWPs and analyzing atmospheric circulations. The data have a horizontal  
232 resolution of 2.5°×2.5°, with 144×73 horizontal grids available every 6 hours. From the near surface  
233 layer to 10 hPa, there are 17 pressure levels in the vertical direction. The data of the geopotential  
234 height and wind at 500 hPa and 850 hPa, the vertical wind ( $\Omega$ ), T and RH are used in this study. At

235 the same time, the lowtotal cloud cover (LTCC), the total cloud liquid water (TCLW) and solar  
236 radiation (SR) from ERA-interim are supplemented in this study, which have the same temporal and  
237 spatial resolutions as the FNL data. Moreover, the western Pacific subtropical high index (WPSHI)  
238 and the eastern Asian summer monsoon index (EASMI) are calculated using the FNL data of the  
239 geopotential height and wind at 850 hPa. The WPSHI is defined following theaeaccording to western  
240 Pacific subtropical high intensity index in the National Climate Center of China. Specific formula  
241 refers to website ([https://cmdp.ncc-cma.net/extreme/floods.php?product=floods\\_diag](https://cmdp.ncc-cma.net/extreme/floods.php?product=floods_diag)). The EASMI  
242 is a shear vorticity index. It is defined as the difference of regional mean zonal wind at 850 hPa  
243 between 5 and 15°N, 22.5 and 32.5°N, 90 and 130°E, and 110 and 140°E in Wang and Fan (1999),  
244 recommended by Wang et al. (2008).

域代码已更改

带格式的: 字体颜色: 文字 1

245 The FNL geopotential height field at 850 hPa can capture the synoptic circulation variations  
246 over the YRD well (Shu et al. 2017). In this study, we use the geopotential height at 850 hPa from  
247 April to September during 2014–2018 as the input for the PTT. WPSHI and EASMI are correlated  
248 discussed the correlations with the O<sub>3</sub> time series. WBesides, when we used the Pearson correlation  
249 coefficient to calculate the correlations between two time series, Pearson correlation coefficient is  
250 as the only method to be used.

251

## 252 **2.6. Reconstruction of O<sub>3</sub> concentration based on SWP**

253 To quantify the inter-annual variability captured by the variations (frequency and intensity) in  
254 the synoptic weather patterns, Yararl (1992) provided an algorithm to find the contribution of SWP  
255 frequency variation to the inter-annual O<sub>3</sub> variation. The specific calculation is as follows.

256 
$$\overline{\overline{O_{3m}}}(fre) = \sum_{k=1}^6 \overline{O_{3k}} F_{km} \quad (12),$$

257 where  $\overline{\overline{O_{3m}}}(fre)$  is the reconstructed mean O<sub>3</sub> concentration influenced by the frequency variation  
258 in SWPs from April to September for year  $m$ ,  $\overline{O_{3k}}$  is the 5-year mean O<sub>3</sub> concentration for SWP  
259  $k$ , and  $F_{km}$  is the occurrence frequency of SWP  $k$  during April–September for year  $m$ .

260 –Hegarty et al. (2007) suggested that changes in the SWP include both frequency change and  
261 intensity change. The intensity of SWPs represents the location and strength of the weather system.  
262 Moreover, they noted that the environmental and climate-related contributions to the inter-annual  
263 variations of O<sub>3</sub> could be better separated by considering these two changes. So, Equation12 is

264 modified into the following form.

265  $\overline{O_{3m}}(fre + int) = \sum_{k=1}^6 (\overline{O_{3k}} + \Delta O_{3km}) F_{km}$  (13),

266 where  $\overline{O_{3m}}(fre + int)$  is the reconstructed average  $O_3$  concentration influenced by the frequency and intensity changes of SWPs from April to September for year  $m$ ;  $\Delta O_{3km}$  is the modified difference on the fitting line, which is obtained through a linear fitting of the annual  $O_3$  concentration anomalies ( $\Delta O_3$ ) to the SWP intensity index (SWPII) for SWP  $k$  in year  $m$ .  $\Delta O_{3km}$  represents the part of the annual observed  $O_3$  oscillation caused by the intensity variation in each SWP. Hegarty et al. (2007) used the domain averaged sea level pressure to represent the circulation intensity index (CII). Liu et al. (2019) reconstructed the inter-annual  $O_3$  level in the northern China using the center pressure of the lowest pressure system. However, But we find the intensity variation in each SWP is different when  $O_3$  increases. So we select different SWPII under each SWP pattern—according to the characteristics of high  $O_3$  concentration. Lastly, we select the maximum height in zone-1 ( $25^{\circ}\text{N}$ – $40^{\circ}\text{N}$ ,  $110^{\circ}\text{E}$ – $130^{\circ}\text{E}$ ), the maximum height in zone-2 ( $20^{\circ}\text{N}$ – $50^{\circ}\text{N}$ ,  $90^{\circ}\text{E}$ – $140^{\circ}\text{E}$ ) and the mean height in zone-3 ( $10^{\circ}\text{N}$ – $40^{\circ}\text{N}$ ,  $110^{\circ}\text{E}$ – $130^{\circ}\text{E}$ ). Especially, zones 1, 2 and 3 were selected in term of location of dominated weather systems under each SWP. Detailed demonstration is introduced in section 3.5.

280

281 **3. Results and discussion**

282 **3.1. Spatio-temporal variations of  $O_3$  in the YRD region**

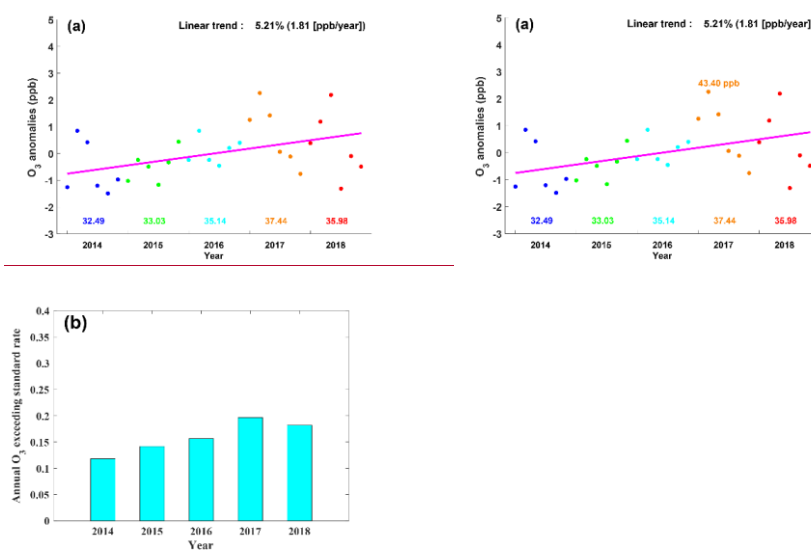
283 **3.1.1. Inter-annual variations of  $O_3$**

284 Fig. 1a shows the time series of the anomalies of the monthly mean  $O_3$  concentration over the  
 285 YRD from April to September during 2014–2018, as well as the corresponding linear fitting curve.  
 286 Fig.~~are~~ 1b shows the annual variation in the total number of days with  $O_3$  concentration exceeding  
 287 the national standard during the warm seasons over 2014–2018 period. As shown in Fig. 1a, the  
 288 monthly mean  $O_3$  concentration in the warm seasons increases over 2014–2018, reaching the  
 289 maximum of 37.44~~37.44~~ ppb in 2017 and maintaining at a high level in 2018. According to the  
 290 generalized least-squares method with auto-regression in section 2.2, obtained fitting function is  
 291  $y_t = -0.8076 + 0.0521t - 0.4824 \cos\left(\frac{2\pi M}{6}\right) + 0.6646 \sin\left(\frac{2\pi M}{6}\right) + R_t$ . Specifically, 5.21%  
 292 (1.81 ppb) of  $k$  value as the  $O_3$  inter-annual variation shows a large increasing trend in the YRD  $O_3$

293 concentration in the YRD shows a large increasing trend of 1.81 ppb (5.21%) per year, which is  
294 slightly higher than that in the entire China (5.00% per year, Lu et al. 2020). Meanwhile, the annual  
295 average days with  $O_3$  exceeding the standard during the warm seasons also show an increasing trend,  
296 reaching a peak in 2017 and maintaining at a high level in 2018. In all, both means and extremes of  
297  $O_3$  concentration have increased over the YRD.

298

299



300  
301 **Fig. 1. (a)** Anomalies of monthly average  $O_3$  concentration from April to September during  
302 2014–2018. The purple solid line represents the linear fitted curve ( $y_t = -0.8076 + 0.0521t$ ),  
303 and the color number represents the annual (April–September) mean of  $O_3$  concentration. (b)  
304 Annual (April–September) variation in the days with  $O_3$  exceeding the national standard.

305

### 306 3.1.2. Characteristics of $O_3$ variability based on the EOF analysis

307 To further discuss the spatio-temporal distribution characteristics of the observed  $O_3$   
308 concentration, the EOF approach is used to uncover the relationship between the spatial distribution  
309 and temporal variation. By removing the missing data for 17 days,  $O_3$  concentrations in 898 days  
310 are processed. The percentages of variance contribution for the first three patterns are 65.70 %,  
311 13.80 % and 9.10 %, respectively. The significance tests of the EOF eigenvalue confirm that the

312 first three patterns are significantly separated. Approximately 88.60 % of the variability in the  
313 original data is contained in these three patterns. In the first EOF pattern (EOF1), the observed O<sub>3</sub>  
314 over the YRD changes similarly and the center of the variation is located in the middle of the YRD  
315 (Fig. 2a). As shown in Fig. 2b, the time series of EOF1 presents an increasing-decreasing-trend  
316 and shows a high negative correlation with the time series of O<sub>3</sub> ( $R = -0.983$ ). Therefore, to some  
317 extent, the EOF1 time series variation can represent the daily mean O<sub>3</sub> variation and implies an  
318 increasing trend of regional mean O<sub>3</sub> concentration during these periods. Considering the negative  
319 values in EOF1, the EOF1 time series implies an increasing trend of regional mean O<sub>3</sub> concentration.  
320 FurthermoreIn addition, we investigated the relationships between the time series of EOF1 and  
321 different weather systems, as well as the meteorological factors have been investigated. Weather  
322 systems include the WPSH and the East Asian summer monsoon, which are dominant weather  
323 systems affecting the YRD. Both of them show a poor correlation with the EOF1 time series ( $R_{WPSH} = -0.133$   
324 and  $R_{EASM} = -0.04$ ). It indicates that the daily O<sub>3</sub> variation is too complex to be  
325 comprehensively explained through the change in a single weather system. Furthermore, the RH  
326 and SR presents a good correlation with the EOF1 time series ( $R_{RH} = -0.59$  and  $R_{SR} = 0.56$ ). Han et  
327 al. (2020) also found that RH is the most important factor affecting O<sub>3</sub> in the YRD. However, it is  
328 still unclear how the change in different weather systems causes the variation in RH and SR, and  
329 how the variations in RH and SR variation impacts the other meteorological factors and O<sub>3</sub>  
330 accumulation.

331 In the second EOF pattern (EOF2), there is obvious east-west contrast. In contrast, the third  
332 EOF (EOF3) pattern presents a notable south-north contrast. At the same time, the increasing trend  
333 of EOF2 time series and the decreasing trend of EOF3 time series indicate that O<sub>3</sub> concentrations in  
334 the west and northwest have risen from 2014 to 2018. It implies that a higher rate of O<sub>3</sub> increasing  
335 would occur in the northwest. As known, the variance contribution of EOF1 is 65.70 % that is  
336 greater than EOF2 (13.80 %) and EOF3 (9.10 %). Therefore, increases in the O<sub>3</sub> increasing in the  
337 entire whole-YRD region is the main trend.

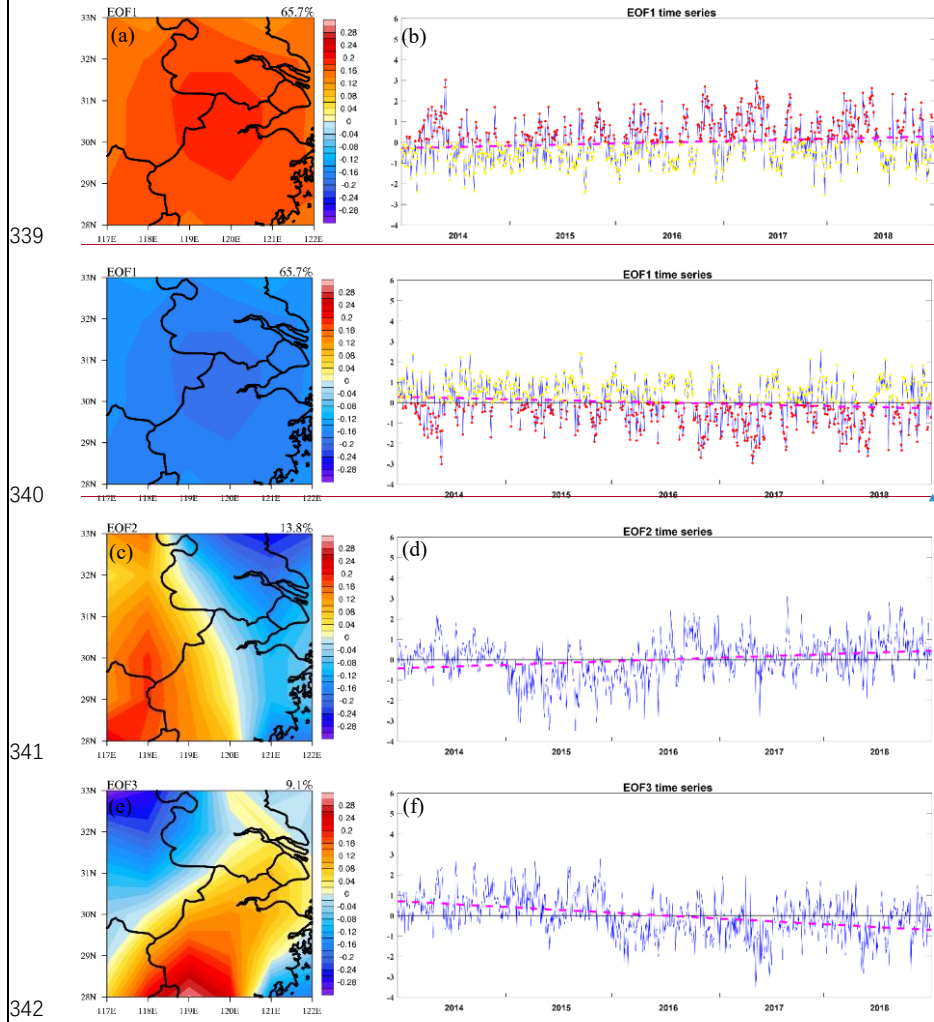
338

带格式的: 非突出显示

带格式的: 非突出显示

带格式的: 非突出显示

带格式的: 非突出显示



339  
340  
341  
342  
343 **Fig. 2. Three EOF patterns of O<sub>3</sub> concentration in the warm seasons from 2014 to 2018,**  
344 including the spatial pattern (a, c and e) and time coefficient (b, d and f). The percentage in  
345 panels (a, c and e) is the variance contribution of each EOF mode. The **pinkorange** dash line  
346 in panels (b, d and f) represents the linear fitted curve.

347  
348 **3.2. Effects of meteorological conditions on O<sub>3</sub> concentration over the YRD region**  
349 **3.2.1. Quantifying the effects of meteorological conditions**  
350 With the primary pollutant emissions being cut down, the surface O<sub>3</sub> increase in the recent years

带格式的: 行距: 单倍行距

带格式的: 字体颜色: 蓝色

351 in China might be attributable to affected by a variety of factors, one of which was suggested to be  
352 the slowing down sink of hydroperoxy radicals, related to the variation in PM<sub>2.5</sub> (Li et al. 2019). Yet,  
353 it is uncertain how meteorological conditions influence the is increasing trend in surface O<sub>3</sub>. Yang et  
354 al. (2019) quantified the meteorological impact on O<sub>3</sub> variation over the Pearl River Delta region  
355 using the meteorological adjustment. Using Similarly to the methodology similar to that in Yang  
356 et al. (2019), we investigate the meteorological influences on the increase in ozone increase over  
357 the YRD in the warm seasons during 2014–2018. Fig. 3a shows the ambient O<sub>3</sub> variation from 2014  
358 to 2018: i.e. O<sub>3</sub> concentration increases from 2014, reaches the maximum in 2017, and maintains  
359 at a relatively high level in 2018. After the meteorological adjustment, the variable increasing  
360 magnitude is lower than the original one, implying that if the meteorological conditions remained  
361 unchanged over the 5 years, the variation variable increasing in magnitude of ambient O<sub>3</sub>  
362 concentration would be lower. The meteorological impact can be examined from the difference  
363 between the black solid and dashed lines in Fig. 3a. it is shown that –We focus on periods from  
364 the middle of 2014 to the middle of 2018 when the difference is negatively from the middle of 2014  
365 to the middle of 2016 and positively large from middle of 2016 to the middle of 2018. In 2017,  
366 the meteorological conditions increase the O<sub>3</sub> concentration by about 1.1620 ppb. However, in 2015,  
367 the meteorological conditions become unfavorable to the O<sub>3</sub> accumulation, leading to an O<sub>3</sub>  
368 reduction of 1.3940 ppb. The meteorological conditions make a difference in changed the O<sub>3</sub>  
369 concentration by 3.032.81 ppb at most between the most favorable year (2017) and the most  
370 unfavorable year (2015), which roughly corresponds to 8.709.62%  
371 
$$\left( \frac{\max(\text{MEO impact}) - \min(\text{MEO impact})}{\text{O}_3(5 \text{ year average})} \right)$$
 of the annual O<sub>3</sub> concentration.

372 In addition, we select the most influential meteorological factors to discuss their impacts on O<sub>3</sub>  
373 variation, including T<sub>2</sub>, RH, sunshine duration, SR, LCC and WS and wind speed. As shown in Fig.  
374 3b, RH is the most crucial factor and its variation is similar to the variation in the total  
375 meteorological impact. In addition, SR and LCC also play important roles and have elose large  
376 impacts impacting on O<sub>3</sub> variation. It indicated that RH can impact s on O<sub>3</sub> concentration  
377 in through two ways. One is gas phase H<sub>2</sub>O reacting with O<sub>3</sub> (O<sub>3</sub> + H<sub>2</sub>O(gas) + hν → O<sub>2</sub> + 2OH).  
378 The other is its influencing on clouds and thereby shielding SR. The East Asian summer monsoon  
379 plays a key role in affecting the local RH, and meanwhile it might bring a certain amount of O<sub>3</sub> from

带格式的: 非突出显示

带格式的: 非突出显示

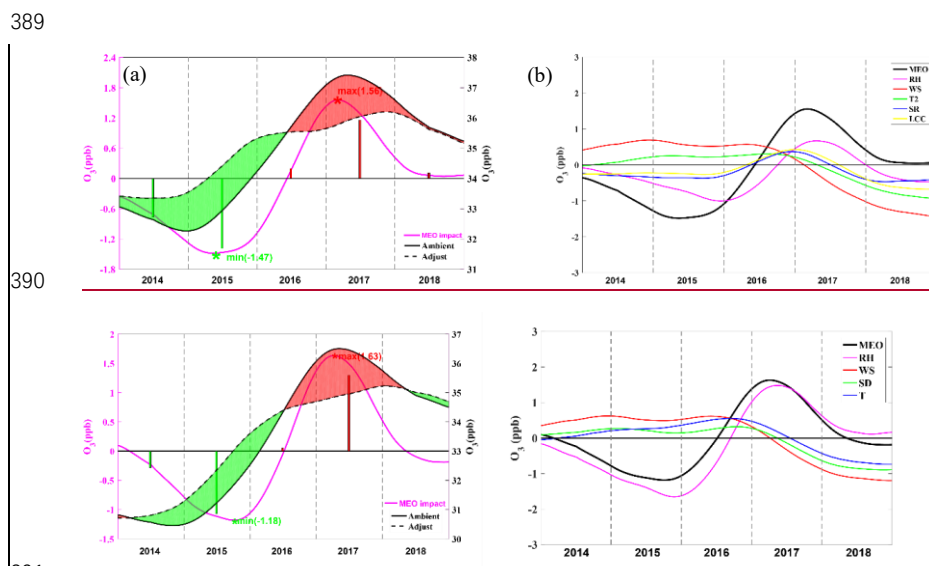
带格式的: 字体颜色: 文字 1

380 the areas south of the YRD area. However,  $O_3$  concentration is high negatively related to RH, which  
 381 implies that the local chemical reaction might contribute to the  $O_3$  accumulation more than the  
 382 regional transport. The impacts of T2 and WS contributions of other two factors are inconsistent with  
 383 the overall sum meteorological impact contribution. Han et al. (2020) also found that RH is the most  
 384 influential factor in the central and south parts of eastern China. The East Asian summer monsoon  
 385 plays a key role in affecting the local RH, and meanwhile it might bring a certain amount of  $O_3$  from  
 386 the south area. However,  $O_3$  concentration is highly negatively related to RH, which implies that the  
 387 local chemical reaction might contribute more to the  $O_3$  accumulation than the regional transport.  
 388 The contributions of the other three factors are relatively insignificant.

带格式的: 非突出显示

带格式的: 非突出显示

带格式的: 非突出显示



390  
 391 Fig. 3. (a) 5-year trends of ambient  $O_3$  (solid black line), meteorological adjusted  $O_3$  (dashed  
 392 black line), and the meteorological impact (pink line) over the YRD during 2014–2018. Periods  
 393 with positive and negative meteorological impacts are shaded in with red and green,  
 394 respectively; red and green bars represent the the- $O_3$  increasesing and decreases attributable  
 395 toing caused by meteorological influences in each year. (b) 5-year variations in the  
 396 meteorological impact of different meteorological factors (MEQR), including relative  
 397 humidity (RH), sunshine duration solar radiation (SR), air temperature (T2), and wind speed  
 398 (WS) and low cloud cover (LCC).

400

401 **3.3. Dynamic processes of O<sub>3</sub> variation driven by synoptic circulations**

402 As discussed in section 3.2, the local meteorological factors have a large great impact on the  
403 O<sub>3</sub> variation. However, to some extent, the variation in local meteorological factors is largely  
404 affected by the synoptic-scale weather circulations (Leibensperger et al. 2008; Fiore et al. 2003;  
405 Wang et al. 2016). For example, in summer the YRD is under a hot-wet environment controlled by  
406 the WPSH. While in winter it is under a cold-dry environment affected by the northwesterly flow  
407 caused by the Siberian High. The different weather systems under their corresponding SWPs have  
408 their unique meteorological characteristics. Moreover, even under one SWP, the location and  
409 intensity changes in a specific weather system can cause the changes in local meteorological factors  
410 correspondingly (Gao et al. 2020).

411

412 **3.3.1. The main synoptic weather patterns in the warm season over the YRD**

413 Applying the PTT classification method, nine SWPs are identified for the warm seasons in the  
414 YRD. Due to the relatively large variance, the first dominant five types SWPs are selected, and the  
415 other four SWP types are grouped as ‘other types’.— As shown in Table 1, SWP1, SWP2 and SWP4  
416 are dominant, accounting for 40.66%, 22.84% and 13.99% of the occurrence frequency,  
417 respectively. In contrast, SWP3, SWP5 and other types occur in low frequencies, being are relatively  
418 lower, and their occurrence frequencies are 7.65%, 6.99% and 6.01%, respectively. Specifically,  
419 SWP1 is under control of affected by the southweeasterly flow introduced by the WPSH. SWP2 is  
420 influenced by the northwesterly flow introduced by a persistent continental high pressure. SWP4 is  
421 influenced by the southeasterly flow introduced by the WPSH and a cyclone. SWP3 and SWP5 are  
422 affected by a cyclone and an anticyclone. For SWP1 and SWP4 are, it is with high temperature and  
423 humidity induced affected by the southerly flow. While under But for SWP5, the YRD is with high  
424 temperature and low RH because of the weak northerly flows are weakened and could not  
425 carry which brings insufficient water vapor, the YRD is with high temperature and low RH. SWP2  
426 is with relatively lower temperature. SWP3 is under the control of a cyclone and the strong upward  
427 motion, it is with weak SR and low er T2. In order to avoid overabundance similar figures with  
428 Figs 4–8, Specific figures of atmospheric circulation at 850 hPa under the main five SWPs are would

429 [be provided in the supplementary](#)

带格式的: 字体颜色: 自动设置

430

431 **TABLE 1. The occurrence days and frequency, typical characteristics, regional mean  $\pm$  the**  
432 **standard error for  $T_2$ temperature (T), relative humidity (RH)RH, wind speed (WS)WS and**  
433 **solar radiation (SR)SR** and positive and negative days under each SWP. The  $> 0$  and  $> 0.5$   
434 **represent the value of EOF1 time series more than 0 and 0.5, respectively. The  $< 0$  and  $< 0.5$  is**  
435 **on the contrary.**

Type and number of days (frequency )	Typical characteristic of SWPs	Pos ( $> 0$ and $> 0.5$ )	
		Meteorological factors	Neg ( $< 0$ and $< 0.5$ ) (number of days)
SWP1 372 (41.43%)	Southwesterly flow introduced by WPSH	$T_2$ ( $^{\circ}$ C): 28.38 $\pm$ 4.94 RH (%): 77.98 $\pm$ 10.44 WS (m/s): 7.30 $\pm$ 0.54 SR (W/m $^2$ ): 1606.20 $\pm$ 537.77	<a href="#">17594</a> , <a href="#">11225</a> <a href="#">19475</a> , <a href="#">12542</a>
SWP2 209 (23.27%)	Northwesterly flow introduced by a continuant high pressure	$T_2$ ( $^{\circ}$ C): 26.40 $\pm$ 5.37 RH (%): 73.97 $\pm$ 12.85 WS (m/s): 7.28 $\pm$ 0.51 SR (W/m $^2$ ): 1615.00 $\pm$ 563.20	<a href="#">11097</a> , <a href="#">7357</a> <a href="#">97110</a> , <a href="#">5773</a>
SWP3 70 (7.80%)	an extratropical cyclone	$T_2$ ( $^{\circ}$ C): 25.41 $\pm$ 4.37 RH (%): 86.80 $\pm$ 6.25 WS (m/s): 7.33 $\pm$ 0.58 SR (W/m $^2$ ): 959.73 $\pm$ 478.14	<a href="#">1258</a> , <a href="#">645</a> <a href="#">5812</a> , <a href="#">456</a>
SWP4 128 (14.25%)	Southeasterly flow brought by WPSH and a southern cyclone system	$T_2$ ( $^{\circ}$ C): 29.29 $\pm$ 4.24 RH (%): 78.67 $\pm$ 8.51 WS (m/s): 7.11 $\pm$ 0.56 SR (W/m $^2$ ): 1505.97 $\pm$ 538.96	<a href="#">4682</a> , <a href="#">3058</a> <a href="#">8246</a> , <a href="#">5830</a>
SWP5 64 (7.13%)	The north China anticyclone system	$T_2$ ( $^{\circ}$ C): 28.08 $\pm$ 4.99 RH (%): 73.97 $\pm$ 12.03 WS (m/s): 7.22 $\pm$ 0.45	<a href="#">4023</a> , <a href="#">2414</a> <a href="#">2340</a> , <a href="#">1424</a>

SR (W/m <sup>2</sup> ): 1586.78 ± 479.65			
others	/	/	/
55 (6.12%)			

436

437 **3.3.2. Impacts of SWP change on O<sub>3</sub> concentration variation**

438 We explore the impacts of SWP change on O<sub>3</sub> variation through an analysis combined with  
 439 combining the EOF1 mode. As illustrated in section 3.1.2, the EOF1 mode is the dominant mode,  
 440 and it implies the increase of O<sub>3</sub> in the entire YRD whole area is the main trend. The Regarding  
 441 EOF1 time series is closely correlated to, it has a high correlation coefficient with the regional  
 442 mean O<sub>3</sub> concentration (R = -0.983). In this study, we primarily mainly focus on why O<sub>3</sub>  
 443 concentration increases in the entire YRD region, rather than on why the increases in O<sub>3</sub> differ  
 444 spatially inside the YRD. Therefore, we use the EOF1 time series as a proxy to present the regional  
 445 O<sub>3</sub> concentration. In Table 1, the positive phase (Pos) represents that the EOF1 time series is more  
 446 than 0 and it is not beneficial to the production and accumulation of O<sub>3</sub>. On the contrary, the negative  
 447 phase (Neg) corresponds means the low higher O<sub>3</sub> concentrations. We extract the information by  
 448 comparing Pos Neg with Neg Pos to find the changes in each SWP pattern. Yin et al. (2019)  
 449 explored dominant patterns of summer O<sub>3</sub> pollution and associated atmospheric circulation changes  
 450 in eastern China. Differently from their study, we have analyzed the daily variation in SWPs, and  
 451 thus we an identified obtain the change in atmospheric circulations in a higher temporal resolution more  
 452 precisely.

453 In the five main SWPs, the EOF1 time series show an decrease increase trend during their  
 454 occurrence days in the warm seasons. It means that the five main SWP patterns tend to bring cause  
 455 high ambient O<sub>3</sub> concentration through the changes in the SWPs, which. In addition, the SWP  
 456 change include SWP changes in both frequency and intensity changes. We find that the change  
 457 in SWP intensity frequency change in SWPs has less impacts more significantly on the inter-annual  
 458 variation in O<sub>3</sub> levels than the change in SWP frequency intensity change in SWPs, which is  
 459 consistent with the results of Hegarty et al. (2007) and Liu et al. (2019). This contribution of  
 460 intensity change and frequency change will be further discussed in section 3.4. In the following, we  
 461 will concretely discuss the variation characteristics of the five SWPs and their impacts on the

带格式的: 非突出显示

462 increase of O<sub>3</sub> in the YRD. Especially, we will show atmospheric circulations at 850 hPa and 500  
463 hPa, meteorological factors includinges SR, T2, LCC, TCLW, RH, meridional wind at 850hPa  
464 (V850) and W (vertical velocity) under positive and negative phase of all SWPs, and correlation  
465 coefficients of RH, SR and T2 with EOF1 time series under all SWPs are shown.

466 As shown in the previous study, SR, T2 and RH are dominated meteorological factors and can  
467 have extremely directly impacts on O<sub>3</sub> photochemical formation and loss (Xie et al. 2017; Gao et  
468 al. 2020). ToIn order to the explore the importance and difference of their impacteffects on O<sub>3</sub>  
469 concentrations under differenteach SWPs, we calculate the correlation coefficients between the  
470 EOF1 time series and these meteorological factorsem under each SWP. As shown in table 2 and 3,  
471 when the absolute values of the calculated correlation coefficients under a SWP areare greater than  
472 0.4, the corresponding meteorological factorss present significant changes between Pos phase and  
473 Neg phases. Therefore Consequently, we regard themoneeive of them as the crucial meteorological  
474 factors that impactimpacting on O<sub>3</sub> variation under that SWP. In the end, we find that significantly  
475 decreases ining RH and increases instrengthening SR are the crucial meteorological factors under  
476 SWP1, SWP4 and SWP5. For SWP2, significant decreases inly decreasing RH, increases  
477 instrengthening SR and increasing T are the crucial meteorological factors. For SWP3, significant  
478 ly decreases ining RH is the crucial meteorological factor. Hereinafter, we it would be discussed  
479 variations in-how to lead to crucial meteorological factors variation induced by change in  
480 atmospheric circulations.

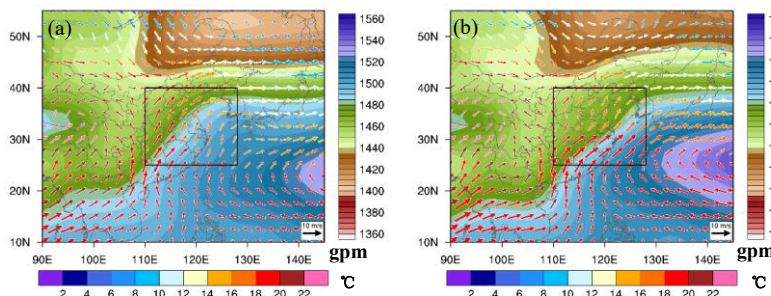
481  
482 **TABLE 2. Correlation coefficient of RH, SR and T2 with EOF1 time series under each SWP.**

Variables	SWP1	SWP2	SWP3	SWP4	SWP5
RH	-0.59	-0.52	-0.50	-0.64	-0.59
SR	0.58	0.56	0.33	0.46	0.48
T2	0.19	0.41	0.26	0.15	0.30

483  
484 Fig. 4 shows the atmospheric circulations at 850 hPa and 500 hPa, and the box plot of  
485 normalizing Table 3 shows meteorological factors includinges SR, T2, TCC, TCLW, RH, meridional  
486 wind at 850hPa (V850) and W (vertical velocity) in table 3 for SWP1\_Pos and SWP1\_Neg. As  
487 shown in Figs. 4a and 4b, the YRD is located at the northwest of the WPSH, mainly affected by the  
488 southwesterly winds. Ceompared with V850 of 4.27 m/s under SWP1\_neg, weakening V850 of

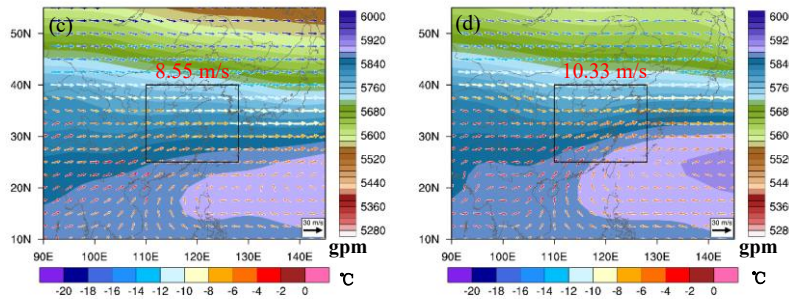
489 2.89 m/s under SWP1\_pos bring a less amount of water vapor to YRD region, therefore, RH shows  
 490 a decrease trend and significantly decreases by 15.24%. Compared with the SWP1\_Pos, the range  
 491 of WPSH is wider in the northwest area under SWP1\_Neg, leading to the strengthened southerly  
 492 wind in the northwest, which results in higher temperature in this area. Due to the weakening of  
 493 V850, the water vapor transport acts in response from the south. RH shows a decrease trend. At 500  
 494 hPa, a shallow trough located at approximate 113°E is replaced by a slowly moving weak  
 495 ridge straight westerly flow, and the downward motion would strengthen and last longer behind the  
 496 shallow trough. The sink motion is favorable for the O<sub>3</sub> accumulation and O<sub>3</sub> photochemical reaction  
 497 at the near surface. Besides, the significantly decreases ining water vaporRH under the downward  
 498 motion condition hindermake the cloud eever hard to formation. LCC and TCLW decreased by  
 499 0.30 and 0.04, respectively. So Furthermore, SR significantly strincreases byonger - 730.04  
 500 W/m<sup>2</sup>solar radiation hits the ground due to the less shelter from of the clouds and less reflection  
 501 above the cloud. Eventually, , further significantly decreases ining RH and increases in strengthening  
 502 SR leading to higher air temperature and stronger O<sub>3</sub> photochemical reaction.

503



504

带格式的: 字体颜色: 自动设置



505  
506 **Fig. 4. The geopotential height (shaded) and 850-hPa wind with temperature (color vector)**  
507 **under (a) SWP1\_Pos and (b) SWP1\_Neg. The geopotential height (shaded) and 500-hPa wind**  
508 **with temperature (color vector) under (c) SWP1\_Pos and (d) SWP1\_Neg. The red values**  
509 **represent the regionally averaged wind speed at 500 hPa in the zone around black lines. (e)**  
510 **The regional average meteorological factors under SWP1\_Pos and SWP1\_Neg, including SR,**  
511 **TCC, 2 m air temperature, RH, meridional wind at 850 hPa (V850) and W (vertical velocity).**  
512 **The boxed area in Figs. 4a-4d encloses the YRD.**

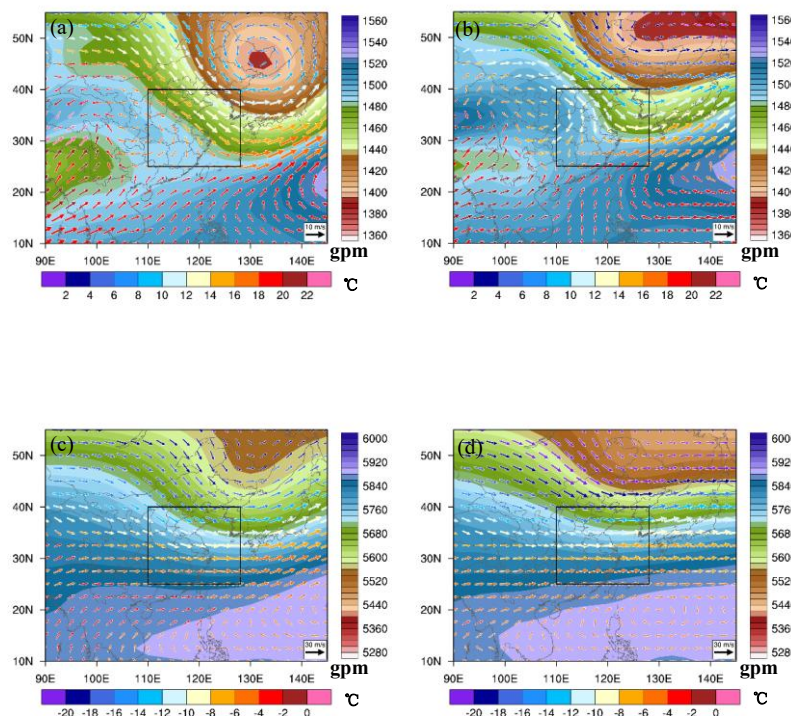
带格式的: 非突出显示

513  
514 Fig. 5 shows the atmospheric circulation structures at 850 hPa and 500 hPa, and Table 3

515 shows meteorological factors including es SR, T, TCC, TCLW, RH, V850 and W in table 3 the box  
516 plot of normalizing factors includes SR, T, TCC, RH, V850 and W for SWP2\_Pos and SWP2\_Neg.  
517 As shown in Figs. 5a and 5b, the YRD is affected by a continental high and the Aleutian low,  
518 characterized by northwesterly flow and a bit southwesterly flow. Compared with the SWP2\_Pos,  
519 the northwesterly flow introduced by the continental high in SWP2\_Neg is weak eniger.  
520 Therefore, So the YRD region is would be influenced by the warm flows and T2 would significantly  
521 increases by 4.91 °C. The correlation between the EOF1 time series and 2 m air temperature T2  
522 under SWP2 ( $R_{SWP2} = -0.41$ ) is closer than the correlation in the whole period ( $R_{all} = -0.24$ ). This  
523 implies that the weakening of the continental high plays an important role in enhancing O<sub>3</sub> there.  
524 Meanwhile, At the same time, as the Aleutian low moves southward slightly, the southwesterly flow  
525 can hardly bring water vapor to the YRD, which leads to RH significantly decreases in RH by  
526 14.79% in this area. The correlation between the EOF1 time series and 2 m air temperature under

527 SWP2 ( $R_{22} = 0.41$ ) is closer than the correlation in the whole period ( $R_{\text{all}} = 0.24$ ). This implies  
 528 that the weakening of the continent high plays an important role in enhancing  $O_3$  there. At 500 hPa,  
 529 a trough located at approximate 120°E–125°E is strengthened associated with Aleutian low shifting  
 530 southward, leading to the stronger downward motion in the northwestern YRD behind the  
 531 strengthening trough. Just like SWP1, stronger downward motion and significantly  
 532 decreasing lower RH enhance strong SR significantly increasing by 790.06 W/m<sup>2</sup> and high air  
 533 temperature. All these changes significantly decreasing RH, strengthening SR and increasing T2  
 534 are beneficial to the  $O_3$  formation and accumulation.

535



536

537  
 538 Fig. 5. The geopotential height (shaded) and 850-hPa wind with temperature (color vector)  
 539 under (a) SWP2\_Pos and (b) SWP2\_Neg. The geopotential height (shaded) and 500-hPa wind  
 540 with temperature (color vector) under (c) SWP2\_Pos and (d) SWP2\_Neg. The red values

带格式的: 字体颜色: 自动设置

带格式的: 字体: (默认) Times New Roman, 非加粗, 字体颜色: 自动设置, 图案: 清除

带格式的: 字体颜色: 自动设置

represent regional average wind speed at 500 hPa in the zone around black lines. (e) The regional average meteorological factors under SWP2\_Pos and SWP2\_Neg, including SR, TCC, 2-m air temperature, RH, meridional wind at 850 hPa (V850) and W. The boxed area in Figs. 5a–5d encloses the YRD.

### 带格式的: 非突出显示

Fig. 6 shows the atmospheric circulations at 850 hPa and 500 hPa, and Table 3 shows and orological factors including SR, T, TCC, TCLW, RH, V850 and W in table 3 the box of normalizing factors includes SR, T, CC, RH, V850 and W for SWP3 Pos and SWP3 Neg.

As shown in Figs. 6a and 6b, the YRD is controlled by an extratropical cyclone. Compared with the SWP3\_Pos, the low pressure in SWP3\_Neg is lower and its location is slightly further eastward SWP3\_Neg. Under this circumstance, the southerly flow at the bottom of the low pressure could hardly bring the water vapor to the YRD and thus RH would significantly decreases by 11.73%. At 500 hPa, the upward motion would be weakening due to the eastern movement of cyclone and western area controlled by back of a strengthening trough located at about 120°E. However, but LCC still is at a high level under upward motion condition. Furthermore, high LCC and its less variation lead to low SR. Therefore, the It is proving that relative low SR-correlation coefficient of 0.33 between SR and with EOF1 time series is relatively low for this SWP3 (r=-0.33). Lastly, only significantly decreasing RH would be crucial factor for and result in high O<sub>3</sub> concentration, the downward motion would be strengthened due to the strengthened trough. The intense downward motion and low RH result in less CC and strong SR, as well as high T, which are instrumental in high O<sub>3</sub> concentration.

带格式的: 字体颜色: 自动设置

带格式的: 字体颜色: 自动设置

带格式的: 字体颜色: 自动设置

带格式的: 字体颜色: 自动设置

带格式的: 字体颜色·自动设置

带格式的·字体颜色·自动设置

带格式的: 字体颜色: 自动设置

带格式的: 字体颜色: 自动设置

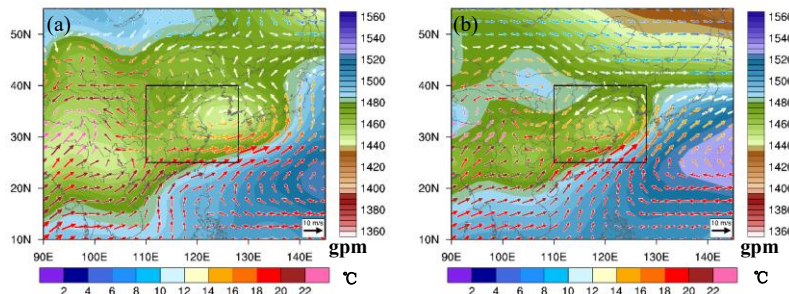
带格式的: 字体颜色: 自动设置

带格式的: 字体颜色: 自动设置

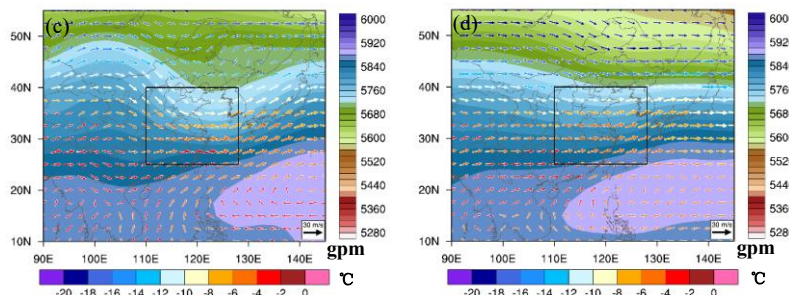
带格式的. 字体颜色. 自动设置

带格式的: 字体颜色: 自动反置

## 带格式的: 非上标/下标



563



564

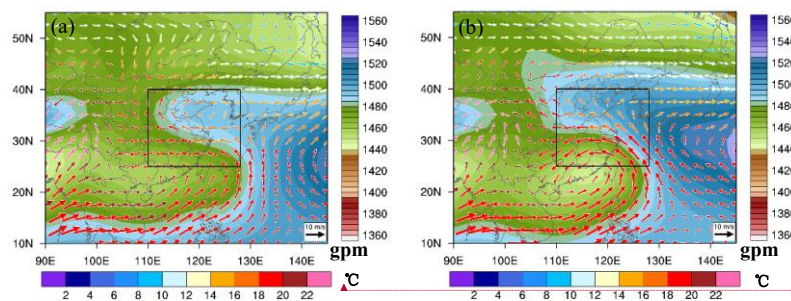
565 **Fig. 6. The geopotential height (shaded) and 850-hPa wind with temperature (color vector)**  
 566 **under (a) SWP3\_Pos and (b) SWP3\_Neg. The geopotential height (shaded) and 500-hPa wind**  
 567 **with temperature (color vector) under (c) SWP3\_Pos and (d) SWP3\_Neg. The red values**  
 568 **represent regional average wind speed at 500 hPa in the zone around black lines. (e) The**  
 569 **regional average meteorological factors under SWP3\_Pos and SWP3\_Neg, including SR, TCC,**  
 570 **2-m air temperature, RH, meridional wind at 850 hPa (V850) and W. The boxed area in Figs.**  
 571 **6a-6d encloses the YRD.**

572

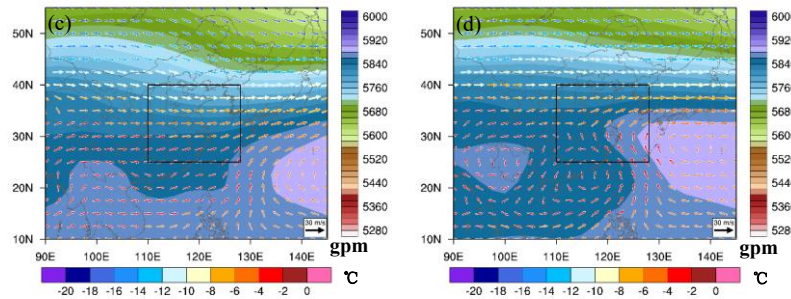
573 Fig. 7 shows the atmospheric circulations at 850 hPa and 500 hPa, and Table 3 shows  
 574 meteorological factors including es-SR, T, LCC, TCLW, RH, V850 and W in table 3 the box plot  
 575 of normalizing factors includes SR, T, TCC, RH, V850 and W for SWP4\_Pos and SWP4\_Neg. As  
 576 shown in Figs. 7a and 7b, the southeasterly wind prevails in the YRD, which is modulated caused

577 by a southern low pressure and the WPSH. Compared with the SWP4\_Pos, the southern low  
 578 pressure and southeasterly flow is weaker in SWP4\_Neg is weaker, and thus it brings less water  
 579 vapor to the YRD and causes RH significantly decreases RHing by 12.26%. At 500 hPa, a shallow  
 580 trough located at about 125°E strengthens associated with weakening of southern cyclone pressure,  
 581 causing the strong sink motion, less LCC and SR of significantly increases in SRing by 538.53  
 582 W/m<sup>2</sup>. Significantly strengthening SR and decreasing RH are important for the O<sub>3</sub> accumulation.  
 583 High temperature, strong SR and low RH caused by the low V850 and downward motion are  
 584 favorable for the O<sub>3</sub> accumulation.

585



586



587

588

589 **Fig. 7. The geopotential height (shaded) and 850-hPa wind with temperature (color vector)**  
 590 **under (a) SWP4\_Pos and (b) SWP4\_Neg. The geopotential height (shaded) and 500-hPa wind**

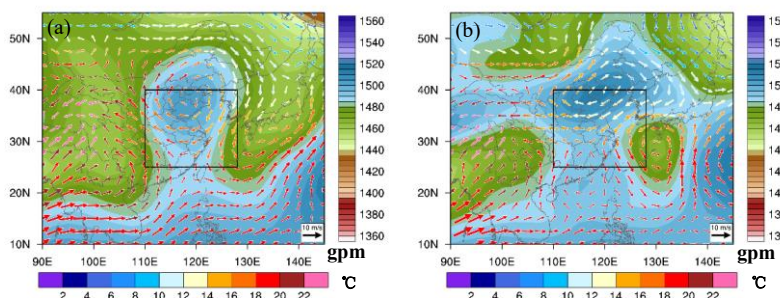
带格式的: 字体颜色: 自动设置

带格式的: 字体: Times New Roman

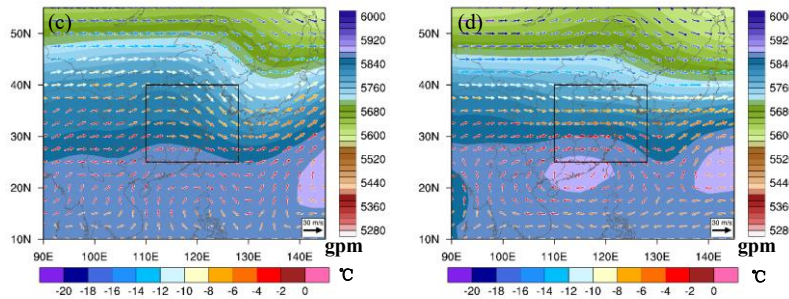
591 with temperature (color vector) under (c) SWP4\_Pos and (d) SWP4\_Neg. The red values  
 592 represent regional average wind speed at 500 hPa in the zone around black lines. (e) The  
 593 regional average meteorological factors under SWP4\_Pos and SWP4\_Neg, including SR, TCC,  
 594 2-m air temperature, RH, meridional wind at 850 hPa (V850) and W. The boxed area in Figs.  
 595 7a-7d encloses the YRD.

596  
 597 Fig. 8 shows the atmospheric circulations at 850 hPa and 500 hPa, and Table 3 shows and  
 598 meteorological factors including SR, T, LCC, TCLW, RH, V850 and W in table 3. the box plot  
 599 of normalizing factors includes SR, T, TCC, RH, V850 and W for SWP5\_Pos and SWP5\_Neg. As  
 600 shown in Figs. 8a and 8b, the YRD is controlled by the north China anticyclone, characterized by  
 601 the northeasterly and the southwesterly winds. Compared with the SWP5\_Pos, the high pressure in  
 602 the SWP5\_Neg is weaker and the northeasterly flow would act in respond accordingly. The  
 603 weakened cold sea flow makes the air warmer and dryer and RH lowers significantly decrease by  
 604 17.34%. At 500hPa, a trough located at about 130°E controlling the YRD would be  
 605 strengthened associated with Japan low pressure appearance. The downward motions  
 606 would become strong correspondingly and result in SR significantly increases in SR by 628.26  
 607 W/m<sup>2</sup>. At last, significantly strengthening SR and decreasing RH lead to increases in the O<sub>3</sub>  
 608 concentration. The favorable for the O<sub>3</sub> accumulation.

609



610



611  
612  
613 **Fig. 8. The geopotential height (shaded) and 850-hPa wind with temperature (color vector)**  
614 **under (a) SWP5\_Pos and (b) SWP5\_Neg. The geopotential height (shaded) and 500 hPa wind**  
615 **with temperature (color vector) under (c) SWP5\_Pos and (d) SWP5\_Neg. The red values**  
616 **represent regional average wind speed at 500 hPa in the zone around black lines. (e) The**  
617 **regional average meteorological factors under SWP5\_Pos and SWP5\_Neg, including SR, TCC,**  
618 **2-m air temperature, RH, meridional wind at 850 hPa (V850) and W. The boxed area in**  
619 **Figs.8a-8d encloses the YRD.**

620  
621 **TABLE 3. Regional mean  $\pm$  the standard error of meteorological factors in Pos and phase**  
622 **and-Neg phases and their difference under each SWP pattern.**

带格式的: 字体: 五号, 加粗

带格式的: 字体: 五号, 加粗

SWP	phase	RH (%)	SR (W/m <sup>2</sup> )	T2 (°C)	LCC	TCLW	V850 (m/s)	W (Pa/s)
	Pos	69.70 $\pm$ 9.69	1970.97 $\pm$ 403.19	29.90 $\pm$ 4.76	0.07 $\pm$ 0.15	0.06 $\pm$ 0.08	2.89 $\pm$ 2.24	0.00 $\pm$ 0.05
P1	Neg	84.94 $\pm$ 6.53	1240.93 $\pm$ 460.18	27.45 $\pm$ 4.78	0.37 $\pm$ 0.27	0.17 $\pm$ 0.14	4.27 $\pm$ 2.73	-0.05 $\pm$ 0.05
	Diff	-15.24	730.04	2.45	-0.30	-0.11	-1.38	0.05
	Pos	66.49 $\pm$ 10.96	1968.41 $\pm$ 377.12	28.81 $\pm$ 4.32	0.07 $\pm$ 0.14	0.06 $\pm$ 0.09	-2.47 $\pm$ 3.09	0.02 $\pm$ 0.05
P2	Neg	81.29 $\pm$ 10.78	1178.34 $\pm$ 479.58	23.89 $\pm$ 5.90	0.48 $\pm$ 0.31	0.19 $\pm$ 0.14	-1.37 $\pm$ 3.21	-0.03 $\pm$ 0.06
	Diff	-14.79	790.06	4.91	-0.41	-0.13	-1.10	0.05
	Pos	76.89 $\pm$ 7.09	1371.42 $\pm$ 605.82	27.83 $\pm$ 2.45	0.34 $\pm$ 0.18	0.21 $\pm$ 0.19	-0.67 $\pm$ 3.43	-0.02 $\pm$ 0.04
P3	Neg	88.62 $\pm$ 5.14	854.96 $\pm$ 395.09	24.77 $\pm$ 4.58	0.58 $\pm$ 0.24	0.31 $\pm$ 0.16	1.93 $\pm$ 3.65	-0.09 $\pm$ 0.06
	Diff	-11.73	516.45	3.06	-0.24	-0.10	-2.60	0.07
	Pos	71.11 $\pm$ 7.15	1882.33 $\pm$ 388.10	30.62 $\pm$ 3.69	0.11 $\pm$ 0.16	0.12 $\pm$ 0.16	0.57 $\pm$ 2.40	0.01 $\pm$ 0.04
P4	Neg	83.37 $\pm$ 6.76	1343.80 $\pm$ 547.50	28.93 $\pm$ 4.19	0.35 $\pm$ 0.24	0.19 $\pm$ 0.19	2.46 $\pm$ 3.60	-0.04 $\pm$ 0.06
	Diff	-12.26	538.53	1.69	-0.24	-0.07	-1.89	0.05
	Pos	68.47 $\pm$ 14.19	1827.46 $\pm$ 447.37	29.60 $\pm$ 5.25	0.07 $\pm$ 0.11	0.09 $\pm$ 0.14	-1.83 $\pm$ 3.42	0.01 $\pm$ 0.04

<u>Neg</u>	<u>85.81+3.45</u>	<u>1199.21+397.17</u>	<u>26.43+3.82</u>	<u>0.43+0.30</u>	<u>0.16+0.09</u>	<u>-2.31+5.25</u>	<u>-0.02+0.04</u>
<u>Diff</u>	<u>-17.34</u>	<u>628.26</u>	<u>3.17</u>	<u>-0.35</u>	<u>-0.07</u>	<u>0.48</u>	<u>0.03</u>
<u>Others</u>	<u>L</u>	<u>L</u>	<u>L</u>	<u>L</u>	<u>L</u>	<u>L</u>	<u>L</u>

623

624 **3.4. Indicators for reconstructing inter-annual O<sub>3</sub> variation affected by synoptic-scale**  
 625 **atmospheric circulation**

626 Due to the similar variations in regional mean O<sub>3</sub> concentration and EOF1 time series, we  
 627 have reconstructed the inter-annual EOF1 time series to replace the regional mean O<sub>3</sub> concentration  
 628 by ~~taking into~~accounting either frequency-variation-only or both frequency and intensity variations  
 629 in SWPs, which are EOF1 time series (Fre) and EOF1 time series (Fre + Int), respectively. The  
 630 observed and reconstructed inter-annual EOF1 time series in 2014–2018 ~~over the entire YRD in the~~  
 631 ~~whole~~ region are shown in Fig. 9. ~~Obviously, the frequency changes in SWPs almost have no impact~~  
 632 ~~on the O<sub>3</sub> variability in the entire YRD. Regarding However, considering the intensity change, the~~  
 633 ~~fitting curve would be closer to the EOF1 time series. ToIn order to obtain the accurate frequency~~  
 634 ~~and intensity change contributions, quantitative evaluation is carried out, we define the contribution~~  
 635 ~~index as the difference between the maximum \_value and the minimum one of a certain~~  
 636 ~~reconstructed time series divided by the difference between the maximum-value and the minimum~~  
 637 ~~value of inter-annual EOF1 time series: Contribution Index = (The reconstructed maximum-value -~~  
 638 ~~the reconstructed minimum-value)/(the original maximum-value - the original minimum-value).~~  
 639 ~~Through the above equation, we deriveget the relative contribution (contribution index) of the~~  
 640 ~~frequency change and the intensive change. Compared with the contribution index of 10.86% for~~  
 641 ~~SWPs frequency change, the value of 48.89% for SWPs intensity change accounts for a larger~~  
 642 ~~proportion. Therefore, the intensity change in SWP is more important to the inter-annual O<sub>3</sub>~~  
 643 ~~variation than the frequency change.~~

带格式的: 字体颜色: 文字 1

带格式的: 字体颜色: 文字 1

带格式的: 字体颜色: 文字 1

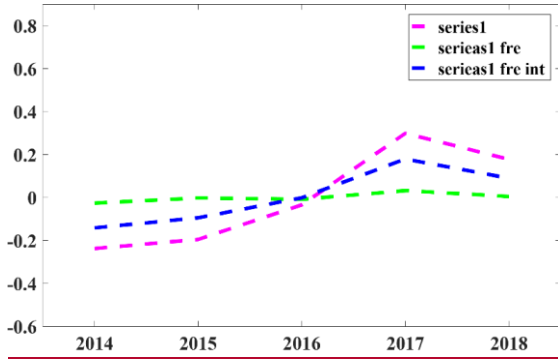
带格式的: 字体颜色: 蓝色

644 ~~Obviously, the frequency changes in SWPs almost have no impact on the O<sub>3</sub> variability in the~~  
 645 ~~entire YRD. Regarding the intensity change, the fitting curve would be closer to the EOF1 time~~  
 646 ~~series. During the reconstructed process, we drastically found that SWPIIs (SWP intensity indexes)~~  
 647 ~~definition play an important role to reconstructing curve. In As previous studies, Hegarty et al.~~  
 648 ~~(2007) and Liu et al. (2019) reconstructed the inter-annual O<sub>3</sub> level in the northeastern United States~~  
 649 ~~and the northern China using the same method as ours. Moreover, They defined the intensity change~~

650 in SWPs using the domain-averaged sea level pressure and the pressure of the lowest-pressure  
651 system. However, As illustrated by Hegarty et al. (2007), but the correlation under Hegarty's Pattern  
652 V is poor, which has negative effect on their reconstructed curve. It indicates we should select the  
653 SWPIIs under each pattern according to their unique characteristics on high O<sub>3</sub> concentration.  
654 Therefore, So we select six SWPIIs and judge their rationality through their correlation  
655 coefficients with EOF1 time series under each SWP: the maximum geopotential heightpressure in  
656 zone 1 (25°N–40°N, 110°E–130°E) and zone 2 (20°N–50°N, 90°E–140°E), the minimum  
657 geopotential heightpressure in zone 1 (25°N–40°N, 110°E–130°E) and zone 2 (20°N–50°N, 90°E–  
658 140°E), and the average geopotential heightpressure in zone 1 (25°N–40°N, 110°E–130°E) and zone  
659 3 (10°N –40°N, 110°E–130°E). As shown in Table 2, for SWP3 and SWP5, the SWPII for the  
660 maximum geopotential heightpressure in zone 1 has a relative high correlation between SWP3 and  
661 SWP5. For SWP1 and SWP4, and the SWPII for the maximum geopotential heightpressure in zone  
662 2 has a relative high correlation between SWP1 and SWP4. we found that The annual EOF1 time  
663 series anomalies the maximum geopotential height show a relatively close good correlation with the  
664 annual EOF1 time series the maximum pressure. It is. It is because the maximum geopotential  
665 heightpressure reflects the wind speed affecting the water vapor transport under this pattern.  
666 Compared with SWP3 and SWP5, the synoptic weather systems are larger than the classification  
667 region for SWP1 and SWP4. So it shows So it can represent better correlation coefficients the  
668 SWPII more precisely in the large zone 2 than in zone 1 under SWP1 and SWP4 region. Under For  
669 SWP2, when O<sub>3</sub> concentration tends to be at a high level, a cold continental high behind the YRD  
670 would tends to weaken. Therefore, we select the average geopotential heightheight in zone 3 to  
671 represent the SWPII under SWP2. From Table 42 shows that, we can know the it has better  
672 reconstructed curve becomes good when we selected different SWPIIs according to the  
673 characteristics of high O<sub>3</sub> level under each patternSWP. Above all, the intensity change in SWP is  
674 more important to the inter annual O<sub>3</sub> variation than the frequency change.

675

676



带格式的: 居中, 缩进: 首行缩进: 0 厘米

677

678 Fig. 9. The trend of the inter-annual EOF1 time series in the warm seasons. The pink curve  
 679 represents the original inter-annual EOF1 time series in the warm seasons, the green line  
 680 represents the reconstructed EOF1 time series only accounting the frequency variation in  
 681 SWPs, and blue line represents the reconstructed ones accounting both the frequency and the  
 682 intensity variations in SWPs.

683 Fig. 9. The original and reconstructed inter-annual EOF1 time series trend based on SWP  
 684 frequency and intensity variations. The pink curve represents the original inter-annual EOF1  
 685 time series, whereas the green and blue lines are the trends of reconstructed inter-annual  
 686 EOF1 time series according to the frequency-variation-only and both frequency and intensity  
 687 variations in SWPs, respectively.

688

689 **TABLE 42. Correlation coefficients between EOF1 time series and different SWPIIs under**  
 690 **each SWP.**

Type	Z <sub>1-ave</sub>	Z <sub>1-max</sub>	Z <sub>1-min</sub>	Z <sub>2-min</sub>	Z <sub>2-max</sub>	Z <sub>3-ave</sub>
SWP1	-0.47	-0.29	-0.35	-0.33	-0.60	-0.32
SWP2	-0.14	-0.08	0.02	-0.07	-0.09	-0.40
SWP3	0.28	0.61	0.03	0.045	0.43	-0.60
SWP4	-0.14	-0.03	-0.17	-0.22	0.78	-0.38
SWP5	0.52	0.76	0.39	0.56	0.72	0.58

691

692 **4. Conclusions and discussions**

693 In this study, we discussed ~~the~~ meteorological influences on the O<sub>3</sub> variation in the warm  
 694 seasons during 2014–2018 in the YRD, China. Specifically, we analyzed the O<sub>3</sub> spatio-temporal  
 695 distribution characteristics, quantified the contribution of meteorological conditions to ~~the~~ O<sub>3</sub>  
 696 variations, explored how ~~the~~ changes in SWPs and corresponding meteorological factors lead to O<sub>3</sub>  
 697 increase in the YRD over 2014–2018, and assessed quantitatively analyzed the contributions  
 698 impact of SWP frequency and intensity to the inter-annual O<sub>3</sub> variation in the region. The main  
 699 conclusions are as follows.

700 The annual meanregionalaveraged O<sub>3</sub> concentrations during the warm seasons averaged  
 701 overfrom2014to2018 in the YRD are 32.49, 33.03, 35.14, 37.44 and 35.98 ppb, respectively, for  
 702 eachyearfrom2014to2018, with a significantly increasing rate of 1.81 ppb year<sup>-1</sup> (5.21% year<sup>-1</sup>).  
 703 MeanwhileAtthesametime, the total number of days on which O<sub>3</sub> concentration exceedings the  
 704 national standard also increases with year in a similar pattern. Through the EOF analysis of O<sub>3</sub> in  
 705 space and time, three dominant modes were identified. The first mode is the most dominant mode,  
 706 accounting for 65.7% of ~~the~~ O<sub>3</sub> variation, suggestingimplying that increasetendenciesinthe  
 707 increasingprevailoverin the entire YRD ~~is~~ ~~the~~ ~~main~~ ~~tendency~~. A high correlation coefficient  
 708 betweentheEOF1timeseriesandRH ( $R_{sh} = 0.59$ ) indicates that RH is the most influential factor  
 709 leadingtotheO<sub>3</sub>increase.

710 We quantified the influence of meteorology on ~~the~~ inter-annual variation and trend of O<sub>3</sub> over  
 711 the YRD from 2014–2018, and found that the influence could lead to a regional O<sub>3</sub> increase by

带格式的: 非突出显示

带格式的: 下标

带格式的: 下标

712 3.032.81 ppb at most. Especially, compared to SR and LCC of relatively large impacting on O<sub>3</sub> variation, RH plays the most important role in modulating the inter-annual O<sub>3</sub> variation, followed by SR and LCC. It indicated that RH impacts on O<sub>3</sub> concentration through two ways. One is gas phase H<sub>2</sub>O reacting with O<sub>3</sub> (O<sub>3</sub> + H<sub>2</sub>O(gas) + hν → O<sub>2</sub> + 2OH). The other is its influencing on clouds and thereby shielding SR. To Moreover, in order to explore connections between the O<sub>3</sub> variation and synoptic circulations, we further identified nine types of SWPs were objectively identified based on the PTT method, and selected five main types were selected to explore their impact on O<sub>3</sub> variation correlate with the EOF1 time series. The typical weather systems of the five SWPs include the WPSH under SWP1, a continental high under SWP2, an extratropical cyclone under SWP3, a southern low pressure and a WPSH under SWP4 and the north China anticyclone under SWP5. Combining EOF1 time series variation under each SWP, we found that the variation in all SWPs over 2014–2018 are favorable to O<sub>3</sub> increase during that period. The variation in SWP intensity include the WPSH weakening and northward extending under SWP1, a continent high weakening under SWP2. However, the crucial changes in meteorological factors attributable to the increases in causing the increasing of O<sub>3</sub> concentrations are different under each SWP. For SWPs 1, SWP4 and SWP5, the crucial changes in meteorological factors include significant decreases in factors are significantly decreasing RH and increases in strengthening SR, which are predominantly attributable to caused by the WPSH weakening and northward extending under SWP1, the southern low pressure weakening and the WPSH weakening under SWP4, and the north China anticyclone weakening under SWP5. These changes in weather systems prevent the water vapor from being transported to the YRD and result in RH significantly decreased by 15.24, 12.26 and 17.34%, respectively. Moreover, the significant ly decreases in RH and increases in the strengthening downward motion (behind the strengthening trough and in front of the strengthening ridge) lead to less LCC, and thereby SR significantly increases by 730.04, 538.53 and 628.26 W/m<sup>2</sup>, respectively. Under For SWP2, the crucial changes in meteorological factors are significant ly decrease in increasing RH by 14.79%, and increases in strengthening SR by 790.06 W/m<sup>2</sup> and increasing T2 by 4.91 °C. RH significantly decreases by 14.79%, SR significantly strengthens increases by 790.06 W/m<sup>2</sup> and T2 significantly increases by 4.91 °C. These changes are mainly chiefly induced produced by a continent high weakening, which has a similar

带格式的: 下标

带格式的: 下标

带格式的: 非突出显示

带格式的: 下标

带格式的: 非突出显示

带格式的: 非突出显示

带格式的: 非突出显示

带格式的: 非突出显示

带格式的: 非突出显示

741 influential mechanism between RH, LCC and SR with SWPs 1, 4 and 5. In addition, significantly  
742 increases in T2 would be due to weakening cold flow introduced by a weakening continent high.  
743 Under SWP3, the they are significantly decreases inereasing RH. Under SWP3, RH  
744 significantly decreased by 11.73% is mainly induced by an intensified extratropical cyclone  
745 thatstrengthening blocks the southerly flow carrying water vapor into the YRD. These change are  
746 critical to O<sub>3</sub> formation under each SWP.

747 As the overall change in SWP intensity and that in SWP frequency contribute to Compared  
748 498.89% and of contribution index of SWP intensity change to 110.86% to the changes in of ozone,  
749 we conclude that the change in SWP intensitycontribution index of SWP frequency change, an  
750 extratropical cyclone strengthening under SWP3, the southern low pressure weakening and the  
751 WPSH weakening under SWP4, and the north China anticyclone weakening under SWP5. All these  
752 changes prevent the water vapor from being transported to the YRD and increase air temperature in  
753 YRD. In addition, the downward motions strengthen in the YRD, which is behind the trough and in  
754 front of the ridge due to the strengthening of the ridge and trough, leading to less cloud cover and  
755 stronger SR. All of these are favorable to O<sub>3</sub> formation and accumulation.

756 ~~it is~~ We found that the change in SWPs intensity is more important to the O<sub>3</sub> increase over  
757 2014–2018 than that in SWPs frequency. We further reconstructed the EOF1 time series by  
758 considering different SWPIIs due to the unique characteristics of each SWP. The results are better  
759 than those in Hegarty et al. (2007) and Liu et al. (2019) who used the same SWPIIs in all SWPs.

760 ~~In summary, this study quantified the inter-annual variation and increasing rate of O<sub>3</sub> in the~~  
761 YRD, China, and explored the connection between SWP variations and the O<sub>3</sub> increase. It provides  
762 an enhanced understanding of response of O<sub>3</sub> variation to changes in SWPs from year to year and  
763 thus this understanding may be insightful to planning strategies for O<sub>3</sub> pollution control.

764

#### 765 Authorship contribution statement

766 **Da Gao:** Conceptualization, Data curation, Formal analysis, Meteorology, Investigation,  
767 software, Writing – original draft, Writing – revision. **Min Xie:** Conceptualization, Methodology,  
768 Writing – revision, Project administration, Funding acquisition. **Jane Liu:** Formal analysis,  
769 Meteorology, Writing – revision. **Tijian Wang:** Formal analysis, Funding acquisition. **Chaoqun**

带格式的: 非突出显示

770 **Ma**: Formal analysis, Meteorology. **Haokun Bai**: Formal analysis, Meteorology. **Xing Chen**:  
771 Formal analysis. **Mengmeng LiMeng**: Formal analysis. **Bingliang Zhuang**: Formal analysis. **Shu**  
772 **Li**: Formal analysis

带格式的: 字体: 加粗

773

#### 774 Declaration of competing interest

775 The authors declare that they have no known competing financial interests or personal  
776 relationships that could have appeared to influence the work reported in this paper.

777

#### 778 Acknowledgements

779 This work was supported by the National Key Research and Development Program of China  
780 (2018YFC0213502, 2018YFC1506404).

781

#### 782 References

783 Barnes, E. A., and Fiore, A. M.: Surface ozone variability and the jet position: Implications for projecting  
784 future air quality, *Geophys Res Lett*, 40, 2839-2844, 10.1002/grl.50411, 2013.

785 Cooper, O. R., Schultz, M. G., Schroder, S., Chang, K. L., Gaudel, A., Benitez, G. C., Cuevas, E., Frohlich, M.,  
786 Galbally, I. E., Molloy, S., Kubistin, D., Lu, X., McClure-Begley, A., Nedelec, P., O'Brien, J., Oltmans, S. J.,  
787 Petropavlovskikh, I., Ries, L., Senik, I., Sjoberg, K., Solberg, S., Spain, G. T., Spangl, W., Steinbacher, M.,  
788 Tarasick, D., Thouret, V., and Xu, X. B.: Multi-decadal surface ozone trends at globally distributed remote  
789 locations, *Elementa-Sci Anthropol*, 8, Artn 23 10.1525/elementa.420, 2020.

790 Day, D. B., Xiang, J., and Mo, J.: Association of ozone exposure with cardiorespiratory pathophysiologic  
791 mechanisms in healthy adults (vol 177, pg 1344, 2017), *Jama Intern Med*, 177, 1400-1400,  
792 10.1001/jamainternmed.2017.4605, 2017.

793 Doherty, R. M., Wild, O., Shindell, D. T., Zeng, G., MacKenzie, I. A., Collins, W. J., Fiore, A. M., Stevenson, D.  
794 S., Dentener, F. J., Schultz, M. G., Hess, P., Derwent, R. G., and Keating, T. J.: Impacts of climate change on  
795 surface ozone and intercontinental ozone pollution: A multi-model study, *J Geophys Res-Atmos*, 118,  
796 3744-3763, 10.1002/jgrd.50266, 2013.

797 Eskridge, R. E., Ku, J. Y., Rao, S. T., Porter, P. S., and Zurbenko, I. G.: Separating different scales of motion in  
798 time series of meteorological variables, *B Am Meteorol Soc*, 78, 1473-1483, Doi 10.1175/1520-  
799 0477(1997)078<1473:Sdsomi>2.0.Co;2, 1997.

800 Fiore, A. M., Jacob, D. J., Mathur, R., and Martin, R. V.: Application of empirical orthogonal functions to  
801 evaluate ozone simulations with regional and global models, *J Geophys Res-Atmos*, 108, Artn 4431  
802 10.1029/2002jd003151, 2003.

803 Gao, D., Xie, M., Chen, X., Wang, T. J., Liu, J., Xu, Q., Mu, X. Y., Chen, F., Li, S., Zhuang, B. L., Li, M. M., Zhao,  
804 M., and Ren, J. Y.: Systematic classification of circulation patterns and integrated analysis of their effects  
805 on different ozone pollution levels in the Yangtze River Delta Region, China, *Atmos Environ*,  
806 <https://doi.org/10.1016/j.atmosenv.2020.117760> 2020.

807 Gao, W., Tie, X. X., Xu, J. M., Huang, R. J., Mao, X. Q., Zhou, G. Q., and Chang, L. Y.: Long-term trend of O<sub>3</sub> in

808 a mega City (Shanghai), China: Characteristics, causes, and interactions with precursors, *Sci Total Environ*,  
809 603, 425-433, 10.1016/j.scitotenv.2017.06.099, 2017.

810 Han, H., Liu, J. E., Shu, L., Wang, T. J., and Yuan, H. L.: Local and synoptic meteorological influences on daily  
811 variability in summertime surface ozone in eastern China, *Atmos Chem Phys*, 20, 203-222, 10.5194/acp-  
812 20-203-2020, 2020.

813 He, J. J., Gong, S. L., Yu, Y., Yu, L. J., Wu, L., Mao, H. J., Song, C. B., Zhao, S. P., Liu, H. L., Li, X. Y., and Li, R. P.:  
814 Air pollution characteristics and their relation to meteorological conditions during 2014-2015 in major  
815 Chinese cities, *Environ Pollut*, 223, 484-496, 10.1016/j.envpol.2017.01.050, 2017.

816 Hegarty, J., Mao, H., and Talbot, R.: Synoptic controls on summertime surface ozone in the northeastern  
817 United States, *J Geophys Res-Atmos*, 112, Artn D14306 10.1029/2006jd008170, 2007.

818 Hou, X. W., Zhu, B., Kumar, K. R., and Lu, W.: Inter-annual variability in fine particulate matter pollution over  
819 China during 2013-2018: Role of meteorology, *Atmos Environ*, 214, ARTN 116842  
820 10.1016/j.atmosenv.2019.116842, 2019.

821 Jacob, D. J., and Winner, D. A.: Effect of climate change on air quality, *Atmos Environ*, 43, 51-63,  
822 10.1016/j.atmosenv.2008.09.051, 2009.

823 Jacob, D. J., and Winner, D. A.: Effect of climate change on air quality, *Atmos Environ*, 43, 51-63, 2009.

824 Jerrett, M., Burnett, R. T., Pope, C. A., Ito, K., Thurston, G., Krewski, D., Shi, Y. L., Calle, E., and Thun, M.: Long-  
825 Term Ozone Exposure and Mortality, *New Engl J Med*, 360, 1085-1095, Doi 10.1056/Nejmoa0803894,  
826 2009.

827 *Jin, X. M., and Holloway, T.: Spatial and temporal variability of ozone sensitivity over China observed from  
828 the Ozone Monitoring Instrument, J Geophys Res-Atmos*, 120, 7229-7246, 10.1002/2015JD023250, 2015.

829 Leibensperger, E. M., Mickley, L. J., and Jacob, D. J.: Sensitivity of US air quality to mid-latitude cyclone  
830 frequency and implications of 1980-2006 climate change, *Atmos Chem Phys*, 8, 7075-7086, DOI  
831 10.5194/acp-8-7075-2008, 2008.

832 Li, K., Jacob, D. J., Liao, H., Shen, L., Zhang, Q., and Bates, K. H.: Anthropogenic drivers of 2013-2017 trends  
833 in summer surface ozone in China, *P Natl Acad Sci USA*, 116, 422-427, 2019.

834 Liu, J. D., Wang, L. L., Li, M. G., Liao, Z. H., Sun, Y., Song, T., Gao, W. K., Wang, Y. H., Li, Y., Ji, D. S., Hu, B.,  
835 Kerminen, V. M., Wang, Y. S., and Kulmala, M.: Quantifying the impact of synoptic circulation patterns on  
836 ozone variability in northern China from April to October 2013-2017, *Atmos Chem Phys*, 19, 14477-  
837 14492, 10.5194/acp-19-14477-2019, 2019.

838 Lu, X., Hong, J. Y., Zhang, L., Cooper, O. R., Schultz, M. G., Xu, X. B., Wang, T., Gao, M., Zhao, Y. H., and Zhang,  
839 Y. H.: Severe Surface Ozone Pollution in China: A Global Perspective, *Environ Sci Tech Let*, 5, 487-494,  
840 10.1021/acs.estlett.8b00366, 2018.

841 Lu, X., Zhang, L., Chen, Y. F., Zhou, M., Zheng, B., Li, K., Liu, Y. M., Lin, J. T., Fu, T. M., and Zhang, Q.: Exploring  
842 2016-2017 surface ozone pollution over China: source contributions and meteorological influences,  
843 *Atmos Chem Phys*, 19, 8339-8361, 10.5194/acp-19-8339-2019, 2019.

844 Lu, X., Zhang, L., Wang, X. L., Gao, M., Li, K., Zhang, Y. Z., Yue, X., and Zhang, Y. H.: Rapid Increases in Warm-  
845 Season Surface Ozone and Resulting Health Impact in China Since 2013, *Environ Sci Tech Let*, 7, 240-  
846 247, 10.1021/acs.estlett.0c00171, 2020.

847 Milancus, M. L., Rao, S. T., and Zurbanco, I. G.: Evaluating the effectiveness of ozone management efforts  
848 in the presence of meteorological variability, *J Air Waste Manage*, 48, 201-215, Doi  
849 10.1080/10473289.1998.10463673, 1998.

850 Papanastasiou, D. K., Melas, D., Bartzanas, T., and Kittas, C.: Estimation of Ozone Trend in Central Greece,  
851 Based on Meteorologically Adjusted Time Series, *Environ Model Assess*, 17, 353-361, 10.1007/s10666-

852 011-9299-6, 2012.

853 Philipp, A., Beck, C., Huth, R., and Jacobbeit, J.: Development and comparison of circulation type  
854 classifications using the COST 733 dataset and software, *Int J Climatol*, 36, 2673-2691, 10.1002/joc.3920,  
855 2016.

856 Pu, X., Wang, T. J., Huang, X., Melas, D., Zanis, P., Papanastasiou, D. K., and Poupkou, A.: Enhanced surface  
857 ozone during the heat wave of 2013 in Yangtze River Delta region, China, *Sci Total Environ*, 603, 807-  
858 816, 10.1016/j.scitotenv.2017.03.056, 2017.

859 Rao, S. T., and Zurbenko, I. G.: Detecting And Tracking Changes In Ozone Air-Quality, *J Air Waste Manage*,  
860 44, 1089-1092, Doi 10.1080/10473289.1994.10467303, 1994.

861 Rao, S. T., and Zurbenko, I. G.: Detecting And Tracking Changes In Ozone Air-Quality, *J Air Waste Manage*,  
862 44, 1089-1092, Doi 10.1080/10473289.1994.10467303, 1994.

863 Santurtun, A., Gonzalez-Hidalgo, J. C., Sanchez-Lorenzo, A., and Zarrabeitia, M. T.: Surface ozone  
864 concentration trends and its relationship with weather types in Spain (2001-2010), *Atmos Environ*, 101,  
865 10-22, 10.1016/j.atmosenv.2014.11.005, 2015.

866 Shu, L., Xie, M., Wang, T. J., Gao, D., Chen, P. L., Han, Y., Li, S., Zhuang, B. L., and Li, M. M.: Integrated studies  
867 of a regional ozone pollution synthetically affected by subtropical high and typhoon system in the  
868 Yangtze River Delta region, China, *Atmos Chem Phys*, 16, 15801-15819, 10.5194/acp-16-15801-2016,  
869 2016.

870 Shu, L., Xie, M., Gao, D., Wang, T. J., Fang, D. X., Liu, Q., Huang, A. N., and Peng, L. W.: Regional severe particle  
871 pollution and its association with synoptic weather patterns in the Yangtze River Delta region, China,  
872 *Atmos Chem Phys*, 17, 12871-12891, 10.5194/acp-17-12871-2017, 2017.

873 Shu, L., Wang, T., Han, H., Xie, M., Chen, P., Li, M., and Wu, H.: Summertime ozone pollution in the Yangtze  
874 River Delta of eastern China during 2013-  
875 2017: Synoptic impacts and source apportionment, *Environ. Pollut.*, 257, 113631, <https://doi.org/10.1016/j.envpol.2019.113631>, 2020.

876 Wang, B., and Fan, Z.: Choice of south Asian summer monsoon indices, *B Am Meteorol Soc*, 80, 629-638,  
877 Doi 10.1175/1520-0477(1999)080<0629:Cosasm>2.0.Co;2, 1999.

878 Wang, B., Wu, Z. W., Li, J. P., Liu, J., Chang, C. P., Ding, Y. H., and Wu, G. X.: How to measure the strength of  
879 the East Asian summer monsoon, *J Climate*, 21, 4449-4463, 10.1175/2008JCLI2183.1, 2008.

880 Teng, L., Zhang, H. L., Yu, J., He, M. M., Xu, N. B., Zhang, J. J., Qian, F. Z., Feng, J. Y., and Xiao, H.: Characteristics  
881 of surface ozone and nitrogen oxides at urban, suburban and rural sites in Ningbo, China, *Atmos Res*,  
882 187, 57-68, 2017.

883 Wang, T., Xue, L. K., Brimblecombe, P., Lam, Y. F., Li, L., and Zhang, L.: Ozone pollution in China: A review of  
884 concentrations, meteorological influences, chemical precursors, and effects, *Sci Total Environ*, 575, 1582-  
885 1596, 10.1016/j.scitotenv.2016.10.081, 2017.

886 Wise, E. K., and Comrie, A. C.: Extending the Kolmogorov-Zurbenko filter: Application to ozone, particulate  
887 matter, and meteorological trends, *J Air Waste Manage*, 55, 1208-1216, Doi  
888 10.1080/10473289.2005.10464718, 2005.

889 Xie, M., Zhu, K. G., Wang, T. J., Yang, H. M., Zhuang, B. L., Li, S., Li, M. G., Zhu, X. S., and Ouyang, Y.: Application  
890 of photochemical indicators to evaluate ozone nonlinear chemistry and pollution control  
891 countermeasure in China, *Atmos Environ*, 99, 466-473, 10.1016/j.atmosenv.2014.10.013, 2014.

892 Xie, M., Liao, J., Wang, T., Zhu, K., Zhuang, B., Han, Y., Li, M., and Li, S.: Modeling of the anthropogenic heat  
893 flux and its effect on regional meteorology and air quality over the Yangtze River Delta region, China,  
894 *Atmospheric Chemistry and Physics*, 16, 6071-6089, 10.5194/acp-16-6071-2016, 2016a.

带格式的: 字体: (默认) Segoe UI Emoji, 小五

带格式的: 字体颜色: 自动设置

896 [Xie, M., Zhu, K., Wang, T., Chen, P., Han, Y., Li, S., Zhuang, B., and Shu, L.: Temporal characterization and](#)  
897 [regional contribution to O<sub>3</sub> and NO<sub>x</sub> at an urban and a suburban site in Nanjing, China. The Science of](#)  
898 [the total environment, 551-552, 533-545, 10.1016/j.scitotenv.2016.02.047, 2016b.](#)

899 [Xie, M., Shu, L., Wang, T.-j., Liu, Q., Gao, D., Li, S., Zhuang, B.-l., Han, Y., Li, M.-m., and Chen, P.-l.: Natural](#)  
900 [emissions under future climate condition and their effects on surface ozone in the Yangtze River Delta](#)  
901 [region, China. Atmospheric Environment, 150, 162-180, 10.1016/j.atmosenv.2016.11.053, 2017.](#)

902 Yang, Y., Liao, H., and Li, J.: Impacts of the East Asian summer monsoon on interannual variations of  
903 summertime surface-layer ozone concentrations over China, *Atmos Chem Phys*, 14, 6867-6879, 2014.

904 Yang, L. F., Luo, H. H., Yuan, Z. B., Zheng, J. Y., Huang, Z. J., Li, C., Lin, X. H., Louie, P. K. K., Chen, D. H., and  
905 Bian, Y. H.: Quantitative impacts of meteorology and precursor emission changes on the long-term trend  
906 of ambient ozone over the Pearl River Delta, China, and implications for ozone control strategy, *Atmos*  
907 *Chem Phys*, 19, 12901-12916, 10.5194/acp-19-12901-2019, 2019.

908 Yarnal, B.: Synoptic Climatology in Environmental Analysis A Primer, *Journal of Preventive Medicine*  
909 *Information*, 347, 170-180, 1993.

910 Yin, Z. C., Cao, B. F., and Wang, H. J.: Dominant patterns of summer ozone pollution in eastern China and  
911 associated atmospheric circulations, *Atmos Chem Phys*, 19, 13933-13943, 10.5194/acp-19-13933-2019,  
912 2019.

913 Yue, X., Unger, N., Harper, K., Xia, X. G., Liao, H., Zhu, T., Xiao, J. F., Feng, Z. Z., and Li, J.: Ozone and haze  
914 pollution weakens net primary productivity in China, *Atmos Chem Phys*, 17, 6073-6089, 10.5194/acp-  
915 17-6073-2017, 2017.

916 Zhang, J. X., Gao, Y., Luo, K., Leung, L. R., Zhang, Y., Wang, K., and Fan, J. R.: Impacts of compound extreme  
917 weather events on ozone in the present and future, *Atmos Chem Phys*, 18, 9861-9877, 10.5194/acp-18-  
918 9861-2018, 2018.

919 Zhao, Z. J., and Wang, Y. X.: Influence of the West Pacific subtropical high on surface ozone daily variability  
920 in summertime over eastern China, *Atmos Environ*, 170, 197-204, 2017.

921